NEURAL NETWORK MODELLING OF THE CREEP PROPERTIES OF STEELS

INTRODUCTION

There is a strong motivation from both an economic and environmental perspective to improve the efficiency of fossil fuel fired power plant. Considering Carnot's machine, the thermodynamic efficiency ρ is proportional to the temperature difference between the cold and the hot sources of water.

$$\rho = \frac{T_h - T_c}{T_c}$$

Since the temperature of the cold source -in most cases, river water- cannot be lower, it is necessary to increase the temperature of the hot source. Today the efficiency of the power plant is limited because of the material used for the steam turbine, which operates at a temperature of about 550°C at a pressure of 30 MPa and for which service duration is about 30 years. An increase in steam conditions from 538°C at a pressure of 30 MPa to 650°C at a pressure of 40 MPa is expected to produce an increase in turbine efficiency of approximately 8% [Takeda and Masuyana, 1991].

It is therefore important to be able to design new steels which can operate at higher temperatures with very good creep properties. The cost of experimentation should be taken into account. An experiment, for economic reasons, cannot last for 30 years. Modelling is a way to reduce the long experimentation and a neural network analysis can take into account the past experience which is copious in power plant steel design. This tool has been exploited in this work to model the behaviour of steel under power plant service conditions and has enabled us to design a new steel which is predicted to have very good creep properties.

CHAPTER ONE

CREEP DEFORMATION

Creep may be defined as the time dependent and permanent deformation of a material when exposed to a constant load. Creep deformation is a thermally activated process and the rate of deformation (creep rate) is extremely temperature sensitive. In metals, creep deformation becomes important beyond $0.4\,T_M$, where T_M is the absolute melting temperature [Reed-Hill and Abbaschian, 1992]. In the case of steel usually used in power plant (9-12% Cr steels), this temperature is approximately 450°C. Clearly power plant materials operate in the temperature regime where creep processes are significant. The creep properties of the materials used limit the operating temperature of many power plant components, such as the turbines. Development of materials with an increased creep resistance is central to the use of power plant with higher temperature and thus with higher efficiency.

a) Creep Mechanisms

Creep deformation can occur by a variety of different mechanisms. The mechanism that dominates depends on the stress and temperature conditions as well as the microstructure of the material. In the case of power plant steels the stress levels are relatively high and the temperatures (compared to the melting point) are relatively low. In this case, creep deformation is controlled primarily by dislocation movement and therefore the thermal energy available for dislocations to overcome obstacles. This type of creep is called power law creep [Frost and Ashby, 1982].

Power law creep involves the movement of dislocations and the creep rate is a result of the balance between work hardening and recovery. Work hardening results in an increased dislocation density, whilst recovery leads to a reduction in dislocation density. If the dislocation density remains constant then the creep rate is given by Norton's Law [Norton, 1929].

$$\dot{\varepsilon} = A(\sigma_a - \sigma_i - \sigma_o - \sigma_c)^n \qquad (1)$$

where σ_a is the applied stress, σ_s, σ_p and σ_g are the internal stresses due to solution, precipitation and grain boundary hardening respectively. For high temperature strength, precipitation hardening is the most important [Bjärbo, 1994]. The most effective method for reducing the creep rate is therefore to form a suitable distribution of particles which are able to act as barriers to dislocation motion.

To determine the optimum particle size and distribution, it is necessary to consider how dislocations overcome barriers to their motion. The barriers presented by the particles may be overcome in three ways [Wachter and Ennis, 1995]:

(i) Orowan Bowing - Dislocation segments bend and pass between adjacent particles. An expanding dislocation loop forms around the particles which meets up and cancels enabling the dislocation to continue its motion. A dislocation ring is left around the particles generating a stress field which adds resistance to the motion of the next coming dislocation. The ease with which dislocation can pass particles by this mechanism increases as the particle spacing increases.

(ii) Particle cutting - When particles are coherent dislocations can cut directly through them.

(iii) Dislocation climb - Dislocations can bypass obstacles by 'climbing' out of their slip plane. This involves the diffusion of vacancies and is therefore easier at higher temperatures.

b) Methods of increasing Creep Resistance

A study of the possible creep mechanisms suggests microstructures which would be expected to have good creep resistance under the conditions used in power plant. In general, creep resistant alloys are based on a matrix which is a solid solution. The presence of misfitting solute atoms in the solid solution makes the passage of dislocations through the matrix more difficult. However, the majority of the creep resistance, at least in the early stage of service is derived from precipitate particles. Ideally, these particles should be small and widely distributed in large numbers throughout the matrix. The particles need to be stable at the temperatures for which the

alloy is designed and to be resistant to coarsening - growth of large particles at the expense of small ones whilst the volume fraction remains constant - as this will reduce their effectiveness as strengtheners.

In power plant steels the formation of carbides (and possibly nitrides) provides the precipitate hardening. Other alloying elements are also present in the matrix and these provide solution hardening.

c) Creep Tests

The creep behaviour of a material may be characterised by a number of different parameters which can be measured by performing the appropriate creep test. For metallic materials most creep tests are conducted in uniaxial tension with dumbbell shaped specimen similar to that used for tensile testing. The tests are carried out at a constant temperature and under either a constant stress or load. A typical creep curve for a metal is shown in Figure 1 :

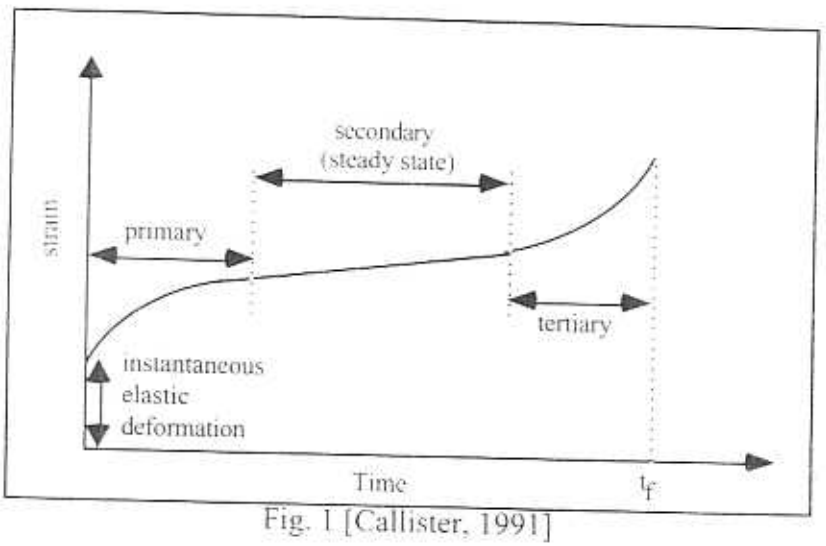

Fig. 1 [Callister, 1991]

The curve may be divided in three regions, primary, secondary and tertiary creep. Primary creep is characterised by a continuously decreasing creep rate. This increase in creep resistance is due to work hardening. Secondary or steady state creep is often the stage of longest duration. The creep rate is constant as a result of the balance between work hardening and recovery processes. Finally for tertiary creep there is an acceleration in the creep rate followed by failure. This failure is termed creep rupture and

may be due to microstructural and/or metallurgical changes; for examples grain boundary separation and the formation of internal cracks, cavities and voids.

For alloy steels such as those used in power plant the real creep curve may be more complex than that shown. This is because in these steels there are microstructural changes which occur throughout the creep test. These changes may include the precipitation of secondary phases which enhance creep resistance (this is known as secondary hardening). There may also be depletion of solute in the matrix by precipitation of coarse phases. This will lead to softening and the creep rate will increase.

The creep parameter that is considered in component design depends on the application. In this work the time to failure is taken into account. It is determined by carried out a creep test at constant load and temperature to the failure point of the material, this is known as a "creep rupture test" and the time of failure is termed the rupture "lifetime".

CHAPTER TWO

THE PHYSICAL METALLURGY OF POWER PLANT STEELS

a) The Fe-Cr-C System

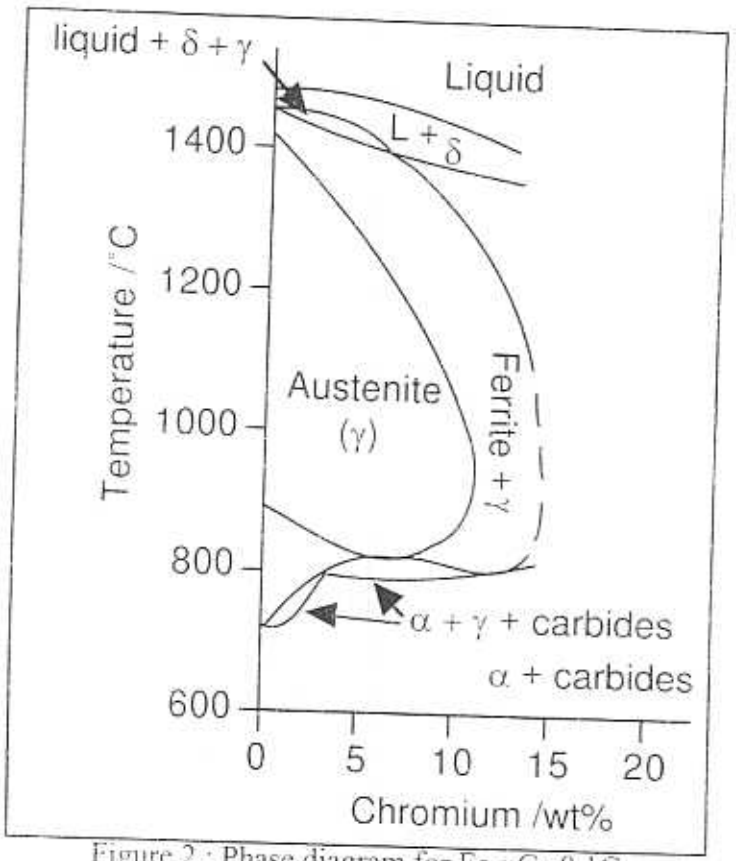

Figure 2 : Phase diagram for Fe-xCr-0.1C
[Sanderson, 1977]

The Fe-Cr-C phase system is complex with the possibility of many different equilibrium phases depending on composition and temperature. This complexity is due to the transition from ferrite stabilising (Fe-Cr) to austenite stabilising (Fe-C) phase regions. Iron may be present either as ferrite (α or δ), austenite (γ), or a mixture of both. There is also the possibility of the formation of a number of different chromium based carbides, some of which have a high solubility for iron. A vertical section through the phase

diagram at 0.1 wt%C is shown in Figure 2. In most steels which have been considered in this work, the equilibrium state between 550 and 650°C is α + carbides.

Adding other elements to the Fe-Cr-C system further increases the complexity of the phase diagram. The majority of alloying elements form carbides (and nitrides if nitrogen is added) to provide precipitation strengthening.

b) Heat treatment

A typical heat treatment for a power plant steel involves austenisation followed by a quench to martensite and subsequent tempering.

During austenisation, the aim is to dissolve all precipitates into the austenite phase without precipitating δ-ferrite which is detrimental to mechanical properties. Precipitates which are not dissolved may coarsen rapidly at the austenitising temperature. The target temperature band may be quite narrow. For example, in studies on a 9Cr-1Mo alloy, Pickering and Vassiliou [1980] have shown that $M_{23}C_6$ carbide does not completely dissolve until 1020°C whilst above 1200°C an increasing quantity of δ-ferrite is formed. Moreover some precipitates such as Nb(C,N) are not dissolved during austenisation [Nickel *et al.* 1995]. Fortunately these particles do not coarsen rapidly and so remain as a fine dispersion in the matrix.

After this austenitisation, the steel is quenched. During quenching, there is insufficient time for the redistribution of substitutional alloying elements and so metastable martensite forms rather than the equilibrium structure (i.e. α-ferrite+carbides). This phase has the same composition as the original austenite and forms because its mechanical transformation does not require diffusion. Unlike ferrite, martensite can be highly supersaturated in carbon which is trapped in the lattice as the martensite forms. This phase can be very hard but is often brittle and therefore almost all technological steels have to be tempered to increase their toughness.

When martensite is heated sufficiently - although not to an extent which would cause reversion to austenite - the trapped carbon is rejected from the solid solution and forms carbides, either with iron or with other alloying elements. The tempering of martensite for power plant steels is usually carried out in the range 660-700°C [Bhadeshia 1992]. The final microstructure consists of a dispersion of carbides within a ferrite matrix which often bears no resemblance to the as-quenched martensite.

c) Phases observed during the tempering of martensite

Many studies have been carried out to identify and characterise the phases observed during martensite tempering [*e.g.* Kuo, 1953 ; Shaw and Quarrel, 1957 ; Baker and Nutting, 1559 ; Woodhead and Quarrel, 1965 ; Yakel, 1985]. This work is summarised for the main phases commonly observed in power plant steels. Typically many alloying elements are soluble in each of these phases to some extent. The chemical formula is therefore often written with "M" representing the total metal content and "X" representing the total C and N content.

According to the studies concerning the tempering of $2^1/_4$Cr1Mo steel of Ballufi *et al.* (1951) and Baker and Nutting (1959), after precipitation of cementite, complex alloy carbides precipitate with complementary dissolution of cementite. These phases may dissolve themselves at later times as different carbides start to precipitate. This latter stage of tempering is of great importance with reference to the creep properties.

M_3C : Called cementite, this phase forms with the composition Fe_3C in iron carbon alloys, but in alloy steels, the partitioning of several alloying elements into the cementite changes the composition significantly. For example, Thomson (1992) has measured chromium levels in excess of 30 wt% in cementite in a $2^1/_4$Cr1Mo steel at 565°C.

M_2X : In many case M_2X is the next phase to precipitate after cementite. The composition can vary widely with molybdenum, chromium and vanadium soluble in significant quantities [Baker and Nutting, 1959 ; Sanderson, 1977]. Precipitation is often accompanied by an increase in the alloy's strength (secondary hardening). In low alloy ferritic steel it is said to be the precipitation of M_2X which is the major factor in conferring creep resistance on the steel.

$M_{23}C_6$: This is a chromium rich carbide which may also contain tungsten, molybdenum, vanadium and nickel [Woodhead and Quarrel, 1965]. In 9-12 wt% Cr steels, it is often the equilibrium carbide and is predominant after typical tempering treatments. It forms after M_2X as large particles and does not directly contribute to creep strength [Bjärbo, 1994].

M_6C : In steels containing molybdenum and relatively low levels of chromium, this is the equilibrium carbide, but as for $M_{23}C_6$, the particles tend to be large and do not enhance creep resistance.

MX : These small spherical precipitates, which may contain titanium, vanadium, and niobium are observed in as-quenched material and are thought to remain

undissolved during austenitisation [Janovec *et al.* 1994]. Moreover, they form a fine dispersion within the martensite laths, and it is therefore thought that they are important in enhancing the creep resistance of steels in which they are present.

Laves phase : It has the general composition Fe_2M where M can be tungsten, molybdenum or some combination of both. V, Ti, Si and Co act as catalysts for Laves phase [Hosoi *et al.* 1986]. Manganese additions are thought to retard the kinetics of Laves phase precipitation [Senior, 1989] and copper may have a benificial effect on its nucleation [Schwind, Hättestrand and Andrén, 1996]. The effect of this phase on creep resistance is currently the subject of much debate.

The usual sequence of phase transformation may be summarised as follows [Baker and Nutting, 1959] :

$$M_3C \dashrightarrow M_3C + M_2X \dashrightarrow M_{23}C_6 \dashrightarrow M_6C$$

Some variations of this sequence can however occur. If Laves phases are equilibrium phases, they form after this sequence. Secondly MX, which forms very stable precipitates, may remain in the alloy during this sequence.

d) Effect of alloying elements on microstructure and creep properties

Alloying additions are made for a variety of purposes. Most are used to stabilise phases which provide creep resistance (*e.g.* M_2X, MX). Elements are also added to provide solid solution strengthening, suppress undesirable phases or for other specific purposes. The effects of the commonly used alloying additions on high temperature microstructure and properties have been reviewed by several authors [Nriggs and Parker, 1965; Greenwell and Beech, 1994]. These effects are summarised below.

Chromium : Ferrite stabilising element and carbide former. Large chromium additions provide hardenability and resistance to corrosion.

Molybdenum : Ferrite stabilising element and carbide former. Stabilises M_2X phase and promotes Laves phases (Fe_2Mo).

Nickel : Austenite stabilising element. Does not normally form carbides. Tends to lead to reduction in creep rupture strength, either by promoting laves phase

[Hosoi *et al.* 1986], or by stabilising M_6C phase which coarsen rapidly [Strang and Vodarek, 1997].

Tungsten : Ferrite stabilising element and carbides former. Stabilises M_2X but less effectively than Mo. Promotes Laves phases. Weak contribution to solid solution strengthening.

Vanadium : Ferrite stabilising element and strong carbide former. Stabilises M_2X phase. May also combine with carbon to form vanadium-rich carbides and carbonitrides (MX).

Niobium : Ferrite stabilising element which forms stable MX precipitates with carbon and nitrogen.

Boron : Considered to be one of the most beneficial elements for high temperature strength. Its addition leads to increase precipitation at grain boundaries.

Carbon : Occupies interstitial sites in both austenite and ferrite, with a greater solubility in austenite which it stabilises relative to ferrite. In practice a carbon level of approximatively 0.15 wt% is the maximum which can be tolerated in power plant steels [Irvine and Pickering, 1969].

Nitrogen : Occupies interstitial sites and is an austenite stabiliser. Increasing nitrogen stabilises M_2X relatively to carbide precipitates.

Copper : Bain and Paxton, in *Alloying elements in steel*, (1961) explain that copper has a maximum solubility of less than 0.3 wt% in ferrite at 600°C. The copper dissolved at elevated temperatures is rejected as nearly pure copper particles at lower temperatures.

e) Microstructural changes during creep deformation

On testing a 10Cr-2W-0.3Mo-0.2 wt% V steel at 600°C the microstructure exhibits two main changes (assuming that it comprises $M_{23}C_6$ and MX precipitates prior to testing) [Vanstone 1994 ; Straub *et al.* 1993 ; Spiradek *et al.* 1994].

(i) Dislocation structure changes. The movement of dislocations is resisted initially by other dislocations because of the reasonably high dislocation density within the martensite laths. Intra-granular particles of MX and the strain fields associated with elements in solid solution also inhibit the motion of dislocations. As creep progresses the uniform dislocation structure within the laths changes as the dislocations start to form sub-grains. This is accompanied by a reduction in the dislocation density [Nickel, 1995].

On further exposure to elevated temperatures the sub-grains tend to grow. The sub-grain boundaries are stabilised by $M_{23}C_6$ and possibly Laves phase formation. As the sub-grains grow the creep rupture strength is reduced and the creep resistance becomes less dependent on the movement of individual dislocations through the matrix and more on the resistance to sub-grain growth.

(ii) Particle distribution changes. As the creep progresses small $M_{23}C_6$ particles on the lath boundaries dissolve and larger $M_{23}C_6$ particles on the block boundaries coarsen. Laves phases also may start to precipitate. The MX precipitates are the most resistant to coarsening and remain as a fine dispersion within the laths.

As seen, a large number of possible phases may precipitate depending on composition and heat treatment. Similarly the creep properties of an alloy are also dependent on these factors.

Ideally the prediction of any model should be explained physically according to the microstructural phenomena described in this chapter.

CHAPTER THREE

NEURAL NETWORK FRAMEWORK

a) linear regression

Most people are familiar with regression analysis, where data are best-fitted to a special relationship which is usually linear. The result is an equation in which each of the inputs x_i is multiplied by a weight w_i.

The sum of all such products and a constant θ then gives the estimate of the output :

$$y = \sum_i w_i x_i + \theta \qquad (2)$$

The weights w_i and the bias θ are chosen in order to minimise the distance between the predictions of the model and the real data. An energy function could be used such as

$$E(w) = \sum_m \left[y^m(w) - t^m \right]^2 \qquad (3)$$

where t^m are the data used for the building of the model and $y^m(w)$ the predicted values with given w_i and θ. The lower $E(w)$, the better is the model for the given data. See Figure 2.

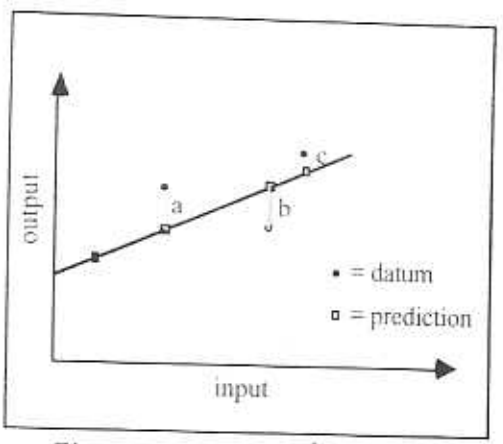

Figure 3 : $E(w) = a^2 + b^2 + c^2$

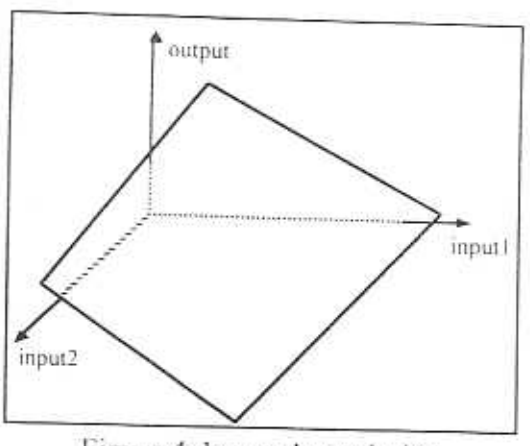

Figure 4: hyperplan solution in case of 2 inputs

Actually, the equation (1) is the equation of an hyperplan in the space whose dimension is equal to the number of inputs plus one (i.e. the output). An example in case of 2 inputs is drawn Figure 3.

This method is simple but can not be applied to a more complicated relationship and there are dangers in using it beyond the range of fitted data.

b) Using of the hyperbolic tangent

In order to model more complicated relationships, some square-terms could be added in equation (1) such as $w_{ij}x_j^2$ or $w_{ij}x_i x_j$ if the product of both variables x_i and x_j has a physical meaning.

An other way to model a non-linear equation is to use the hyperbolic tangent. Indeed, this function is very flexible (Figure 5).

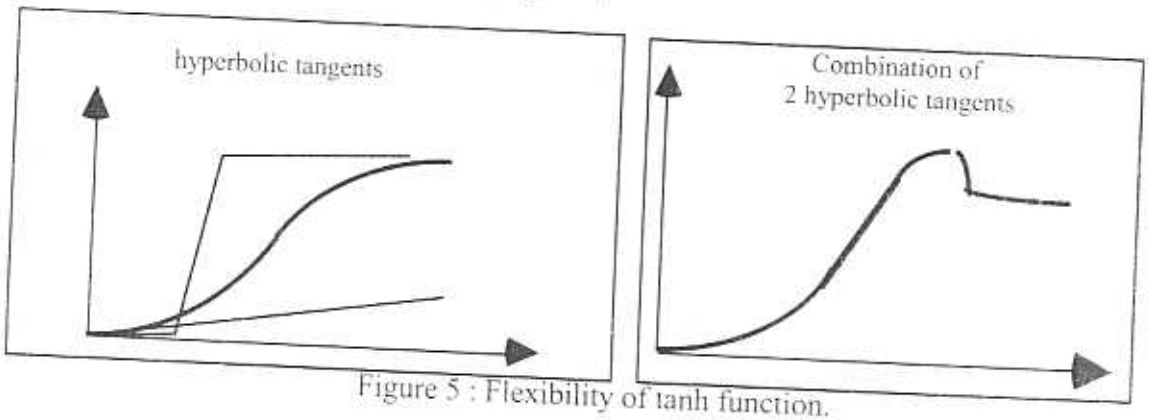

Figure 5 : Flexibility of tanh function.

As before, the input data x_j are multiplied by weights, but the sum of all these products forms the argument of the hyperbolic tangent. The different shape shown in figure 5 are obtained by altering the weight.

This function can be used in a neural network to model some complicated relationships, as in this work with the creep properties in steel.

c) Structure of the neural network.

Figure 6 shows the structure of the neural network used in our model. Factors such as chemical composition, heat treatment, time of rupture and temperature are input from the left hand side. To predict the output, that is, the stress of rupture, hidden units were used between the inputs and the output so that more complex relationships could be expressed. The transfer function relating the inputs to the i th hidden units is given by

$$h_i = tanh\left(\sum_j w_{ij}^{(1)} x_j + \theta_i^{(1)}\right) \tag{4}$$

The relationship between the hidden units and the output is linear:

$$y = \sum_i w_i^{(2)} h_i + \theta^{(2)} \tag{5}$$

The coefficients w and biases θ of these equations are determined in a such way as to minimise an energy function. Because the hyperbolic function is non-linear, a non-linear relationship can be predicted in this model.

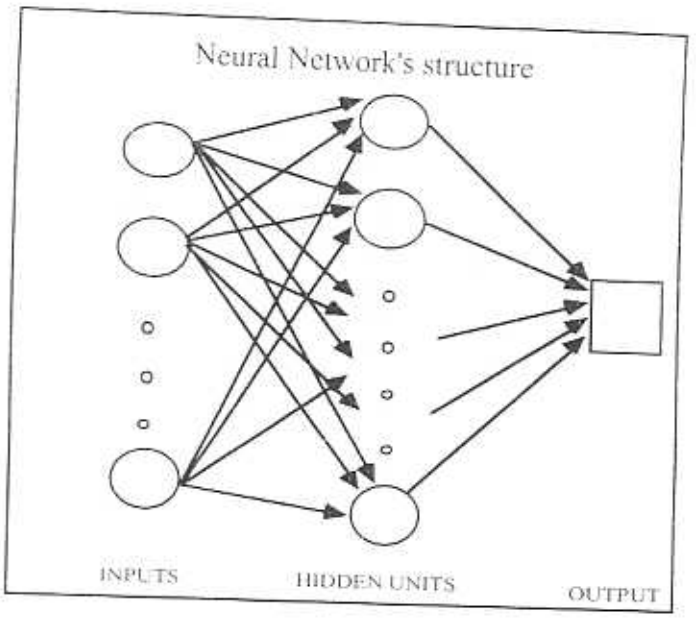

Figure 6.

The stress of rupture was chosen as output because there would be a lot of problems if the time of rupture had been chosen. Indeed for a stress of rupture equal to

zero, the time of rupture is infinite and that is impossible to model with this neural network using hyperbolic tangents.

d) the analysis [D. MacKay, 1992]

Both the input and output variables were first normalised within the range ±0.5 as follows:

$$x_N = \frac{x - x_{min}}{x_{max} - x_{min}} - 0.5 \tag{6}$$

where x_N is the normalised value of x, x_{max} is the maximum value and x_{min} is the minimum value of each variable of the original data. This normalisation is not essential to the neural network approach but allows a convenient comparison of the influence of individual input variables on output.

Using the normalised data, the coefficients (weights) w and bias θ are determined in such a way as to minimise the following energy function:

$$M(w) = \beta E_D + \sum_c \alpha_c E_{w(c)} \tag{7}$$

The energy function consists of the error function, E_D and regularisation E_W The error function is the sum squared error as follows:

$$E_D(w) = \frac{1}{2} \sum_m \left[y(x^m; w) - t^m \right]^2 \tag{8}$$

where $\{x^m, t^m\}$ is the data set. x^m and t^m represent the inputs and the targets respectively. The m is a label of the pair. The coefficients w and biases θ shown in eqs.(2) (4) and (5) make up the parameter vector w. A number of regularisers $E_{w(c)}$ are added to the data error. Each weight is assigned to a class c depending on which neurons it connects with. There is one class associated with each input, one with the hidden unit biases, and one for all weights connected to the output. $E_{w(c)}$ is defined to the sum of the squares of the weights in class c.

$$E_{w(c)}(w) = \frac{1}{2} \sum_{i \in c} w_i^2 \tag{9}$$

This additional term favours small values of w and decreases the tendency of a model to 'overfit' noise in the data set. The control parameters α_c and β together with the number of hidden units determine the complexity of the model. These hyperparameters define the assumed Gaussian noise level $\sigma_v^2 = 1/\beta$ and the assumed weight variances $\sigma_{w(c)}^2 = 1/\alpha(c)\sigma_v$ is the noise level inferred by the model. The parameter

α has the effect of encouraging the weights to decay. Therefore, a high value of σ_w implies that the input parameter concerned explains a relatively large amount of the variation in the output. The values of the hyperparameters are inferred from the data using Bayesian method. Moreover, this method provides 65% confident error bars, which make the prediction very safe.

CHAPTER FOUR
TRAINING OF THE NEURAL NETWORK

a) The database

The database consisted of 2066 combinations of creep rupture stress and, originally, 30 inputs including the time of rupture, chemical composition, temperature, the condition of heat treatment. The contents were given in weight percent, the temperature in Kelvin and the time in hours.

Some modifications were done in this database, using a FORTRAN program named *inbrun.for*, which simultaneously normalised and randomised the data.

(i) Many of the steels were given three steps of heat treatment, normalising, tempering and annealing. For each heat treatment, the temperature, duration and the cooling rate were specified. There were 4 possible cooling methods : furnace, air, oil or water quenching. In cooling rate columns, the number 0, 1, 2, or 3 indicated the kind of cooling rate. This order could have a physical meaning because of an increasing cooling rate, but the proportion between the inputs has not. So, for each heat treatment, one column was created in which 0 or 1 indicated whether or not the corresponding heat treatment was used. When fewer than 3 steps of heat treatment were carried out, the temperature, the duration and cooling rate of the remaining steps were set to zero.

(ii) According to the Arhenius type law which describes the steady-state creep rate [Evans and Wilshire, 1985] :

$$\dot{\varepsilon} = B_1 \exp\frac{-(Q - V\sigma)}{RT} \qquad (10)$$

- where V and B_1 are suitable constants, Q the activation energy for creep, R the gas constant, σ the applied stress and T the temperature - and the experimental rule that steady-state creep rate is inversely proportional to the time of rupture, the logarithm of the time of rupture seemed to have a more significant value than merely the time of rupture. Hence the logarithm in form was used here. This also makes the analysis consistent with the assumption of the neural network that the true function is a continuous function of the inputs.

Table 1 shows the details of the data used for the modelling. The range of chromium content, and the examination of the database showed that values for two types of steels were provided : the $2^1/_4$Cr steel and the ferritic 9-12Cr steel which are usually used in power plant because of their creep resistant properties. This observation indicated that it might be impossible to make good predictions for low-chromium steels because of the lack of relevant experimental data. However, this was not a problem since the most modern creep resistant steels are known to be the ferritic 9-12 Cr steels, and we sought to design steels with this type of composition.

Variable	Range	Mean	Standard Deviation
Log_{10} (creep rupture time)	-0.22 - +5.28	3.021	1.009
Temperature (K)	723 - 977	866.6	61.6
Normalising temperature, K	1123 - 1453	1279	70.42
Duration, hour	0.17 - 33	2.007	3.85
Cooling rate in furnace	0 - 1	0.065	0.248
in air	0 - 1	0.55	0.497
oil quenched	0 - 1	0.256	0.436
water quenched	0 - 1	0.122	0.323
Tempering, Temperature, K	823 - 1133	980	71.8
Duration, hour	0.5 - 32	3.34	5.88
Cooling rate in furnace	0 - 1	0.052	0.223
in air	0 - 1	0.88	0.324
oil quenched	0 - 1	0.032	0.177
water quenched	0 - 1	0.035	0.183
Annealing, Temperature, K	0 - 1023	230.7	404.3
Duration, hour	0.5 - 50	3.96	8.15
Cooling rate in furnace	0 - 1	0.045	0.207
in air	0 - 1	0.955	0.042

Table 1. a

Composition wt%	Range	Mean	Standard Deviation
C	0.004 - 0.23	0.112	0.044
Si	0.01 - 0.86	0.29	0.17
Mn	0.27 - 0.92	0.51	0.11
P	0.001 - 0.029	0.013	0.0076
S	0.001 - 0.02	0.0076	0.0047
Cr	2.17 - 12.9	8.43	3.28
Mo	0.04 - 2.99	0.89	0.513
W	0.01 - 3.93	0.41	0.749
Ni	0.01 - 2	0.24	0.28
Cu	0.01 - 0.87	0.074	0.102
V	0.01 - 0.28	0.119	0.1
Nb	0.005 - 0.312	0.036	0.047
N	0.001 - 0.165	0.031	0.0273
Al	0.001 - 0.057	0.012	0.012
B	0.0003 - 0.051	0.001	0.004
Co	0.008 - 2.5	0.092	0.334
Ta	0.0003 - 0.1	0.0008	0.0069
O	0.003 - 0.035	0.0104	0.0026
Re	0.0003 - 0.6	0.0032	0.0416

Table 1 .b

b) Training of the neural network

One of the dangers of the neural network analysis is the 'overfitting' of data. Indeed, the experimental data always contain error, or noise. The danger involves the modelling of this noise as if it were a physical behaviour (Figure 7).

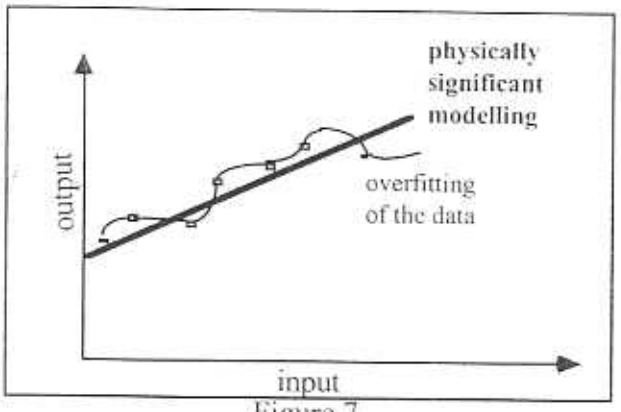

Figure 7

In order to avoid this phenomenon, the database was split in two parts. The first one was used to train the model, the second one to test it. If the neural network overfits the data, it models the random noise and the physical behaviour. In the second part of the database, the physical behaviour is the same but the noise is different. Thus when the model is tested with this part of the database, the test error, that is to say the difference between predicted and previously unseen experimental values, would be larger in the case of overfitting than in the case of a good model. Obviously, the higher the number of hidden units, the more complex is the modelled behaviour, and consequently the risk of overfitting is larger. As observed in the Figure 8. a, beyond 11 hidden units, the test error increased indicating overfitting.

Simultaneously the parameter σ_μ, the difference between predicted and experimental values of the training part of the database decreased continuously, as shown in figure 8. b.

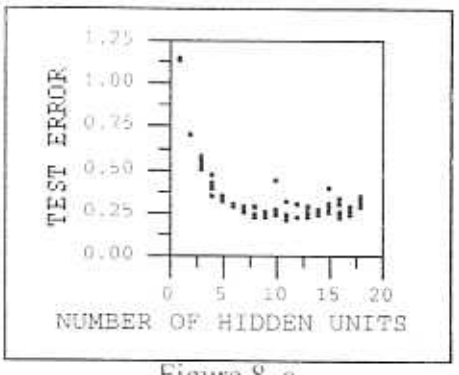

Figure 8. a

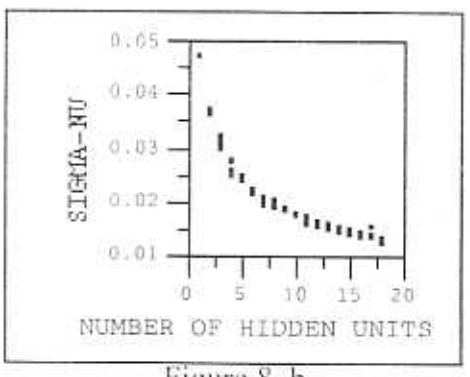

Figure 8. b

c) Committee of models

According to the test error values, the 12 best models were chosen to form a "committee" of models. These best models were combined as follow :

The mean prediction $\bar{y}$ of the committee is

$$\bar{y} = \frac{1}{N}\sum_{i=1}^{N} y_i \qquad (10)$$

and the associated error σ in $\bar{y}$ is given by

$$\sigma^2 = \frac{1}{N}\sum_{i=1}^{N} \sigma_i^2 + \frac{1}{N}\sum_{i=1}^{N} (y_i - \bar{y})^2 \qquad (11)$$

where y_i are the predicted values of each model, and σ_i their error.

Indeed, the random noise has an average equal to zero. By taking into account the mean of the best models, the noise in the experimental values was expected to be reduced.

To choose the best number of models in the committee, the test error of the committees was plotted against the number of models in the committee. It appeared that the committee composed of the 4 best models was the most accurate since it presented the smallest test error, as shown in Figure 9.

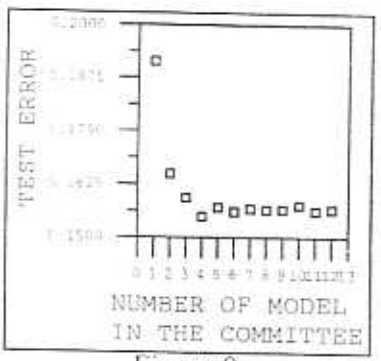

Figure 9

As explained above, overfitting had been avoided by choosing a small number of hidden units and the noise level had been reduced by making a committee of 4 models. So there was no danger in retraining our committee with the whole database in order to improve the model.

As shown in the Figure 10. a , the committee is very accurate, much more so than the single best model (Figure 10. b).

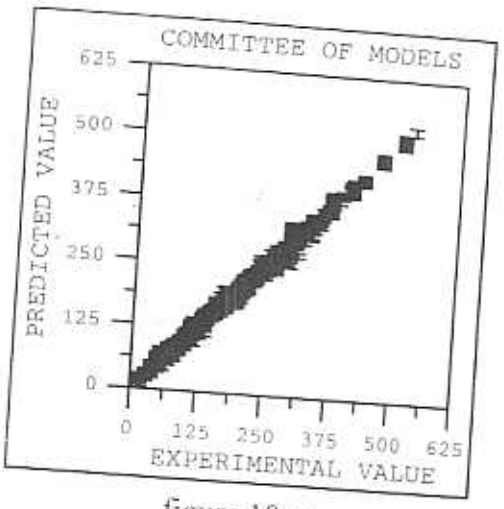

figure 10. a

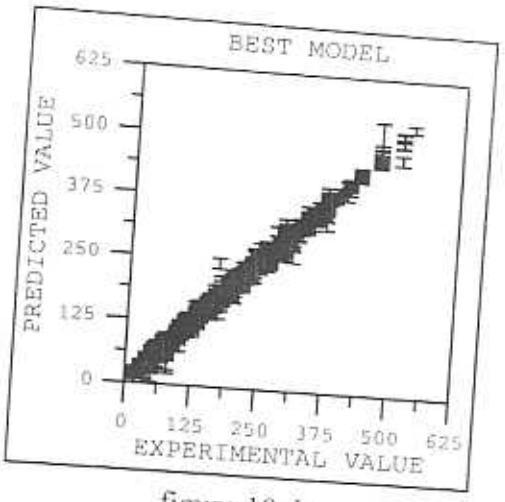

figure 10. b

d) Importance of each input

As seen in the second chapter, the parameter σ_v gives the importance of the variation of the corresponding input. Two phenomena can explain a high value of σ_v :

(i) The corresponding variable physically causes a large variation in the output.

(ii) In the database, a great variation in the output coincides with the variation of the corresponding variable.

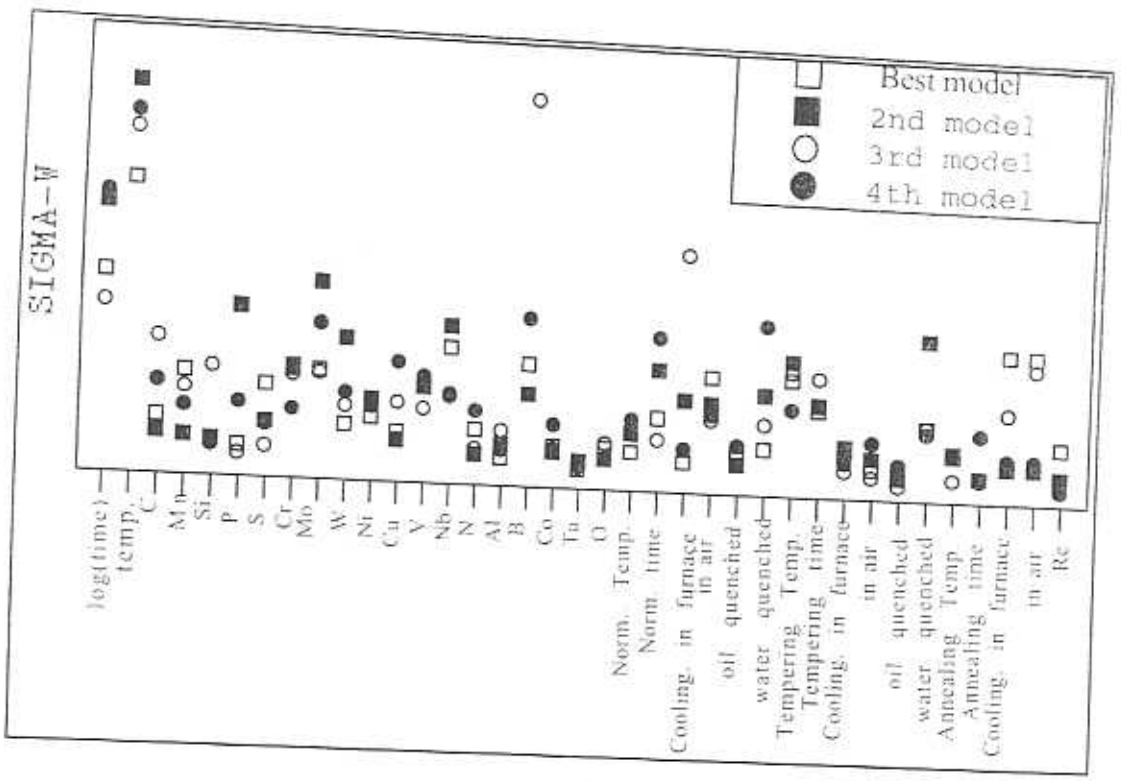

Figure 11

As expected, the temperature and the logarithm of the time seemed to be important variables. The alloying elements chromium, molybdenum, tungsten and niobium had a high significance. But the scattered values of Boron seemed to indicate that no general rule was observed by the neural network for this element.

CHAPTER FIVE
FIRST RESULTS AND LIMITS OF THE MODELLING

a) Evaluation of network performance

In order to test the training of the neural network, two steels were chosen in the database and tested theoretically. The compositions and heat treatments of these steels are written in Table 2.

STEEL	21/4CrMo	10CrMoW
Norm. Temp.	1203K	1338K
Duration, hour	6h	2h
Cooling rate	water q.	in air
Tempering T.	908K	1043K
Duration, hour	6h	4h
Cooling rate	in air	in air
Annealing T.	873°K	1013°K
Duration, hour	2h	4h
Cooling rate	in air	in air
C wt%	0.15	0.12
Si	0.21	0.05
Mn	0.53	0.64
P	0.012	0.016
S	0.012	0.001

STEEL	21/4CrMo	10CrMoW
Cr	2.4	10.61
Mo	1.01	0.44
W	0.01	1.87
Ni	0.14	0.32
Cu	0.16	0.86
V	0.01	0.21
Nb	0.005	0.01
N	0.0108	0.064
Al	0.018	0.022
B	0.0003	0.0022
Co	0.05	0.015
Ta	0.0003	0.0003
O	0.01	0.01
Re	0.0003	0.0003

Table 2

As can be seen in Table 2, both chosen steels are well-known as creep resistant steels. Both $2^1/_4$Cr and 10Cr steels are of the kind usually used in power plant applications [Bhadeshia, 1992; Mayer *et al.*, 1997].

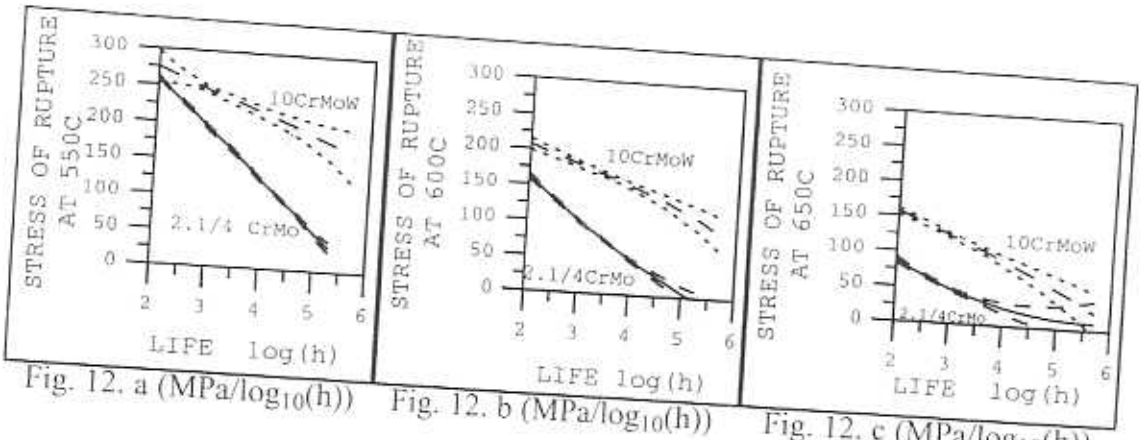

Fig. 12. a (MPa/$\log_{10}$(h)) Fig. 12. b (MPa/$\log_{10}$(h)) Fig. 12. c (MPa/$\log_{10}$(h))

Graphs of stress of rupture vs lifetime were plotted for 3 temperatures, 550°C, 600°C and 650°C. As shown in Figure 12, steels behave in the expected manner : the stress of rupture decreases when the lifetime increases, the $2^1/_4$Cr steel is much less creep resistant than the more recently designed 10CrMoW steel. The error bars which indicate 65% confidence limits are very small when the network is confident of its predictions. The increase in the size of the error-bars at 650°C for longer than 10^4 hours (=about 12 years) lifetime indicates that experimental values are too scarce to enable accurate predictions.

According to these predictions, the neural network seems to be able to predict the behaviour of an already known steel.

b) Analysis of unknown steels

In order to assess the prediction ability of the model, two steels were chosen in a list of creep resistant steels used in power generation and petrochemical industries. Two main behaviours were observed: in the case of compositions similar to these present in the database, the predictions were quite confident (small error bars). If the compositions were quite different from these of the database, the error bars were big and thus the predictions were too uncertain to be used.

The compositions and heat treatments are shown in Table 3, the predictions are presented in Figures 13 a and b.

STEEL	3Cr1.5Mo	9Cr1/2MoW
Norm. temp.	1250K	1338K
Duration, hour	3h	2h
Cooling rate	in air	in air
Tempering T.	950K	1043K
Duration, hour	5h	4h
Cooling rate	in air	in air
Annealing T.	-	1013K
Duration, hour	-	4h
Cooling rate	-	in air
C wt%	0.1	0.11
Si	0.2	0.05
Mn	1	0.45
P	0.005	0.005
S	0.005	0.005

STEEL	3Cr1.5Mo	9Cr1/2MoW
Cr	3	9
Mo	1.5	0.5
W	0.01	1.84
Ni	0.1	0.05
Cu	0.01	0.01
V	0.1	0.2
Nb	0.005	0.07
N	0.001	0.05
Al	0.001	0.001
B	0.0003	0.0003
Co	0.008	0.008
Ta	0.0003	0.0003
O	0.003	0.003
Re	0.0003	0.0003

Table 3

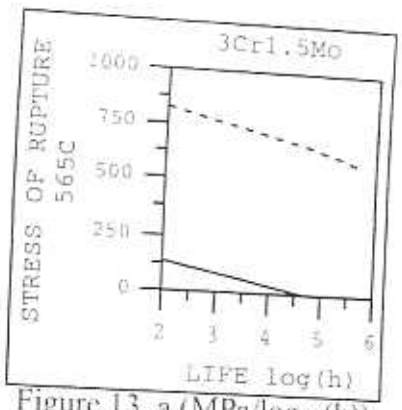

Figure 13. a (MPa/$\log_{10}$(h))

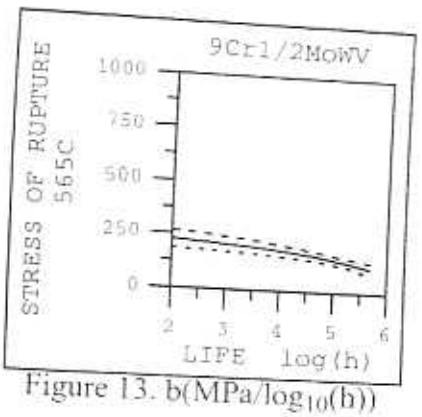

Figure 13. b(MPa/$\log_{10}$(h))

As expected, a composition quite similar to 9Cr$^1/_2$MoW was found in the database (the 10CrMoW steel seen above). Moreover, as described in chapter three, a gap in chromium content was observed between 2.46 and 8.17 wt% which could explain the lack of confidence in the prediction obtained for the 3Cr1.5Mo steel. This example shows

that the neural network is able to reproduce what it has learnt but can not provide good predictions if prior learning of similar physical behaviour has not be done. This underlines the necessity of increasing the number of rows in the database in order to improve the accuracy of the model and to enable it to predict the behaviours of a greater number of steels.

c) Effect of each input

The neural network allows analysis of the effect of each input independently, a procedure that is quite impossible experimentally. However, in most cases this kind of prediction is not very accurate because of a lack of experimental values.

In order to avoid large error bars, each content of the 10CrMoW steel was changed in the range of the database. The stress of rupture was predicted for a time of 10,000 hours and a temperature of 550°C or 600°C. The model was unable to show a convincing tendency for many of the inputs, because of large error bars. In the case of strongly predicted tendencies, physical explanations were sought, in order to prove that the prediction and the model had a physical meaning.

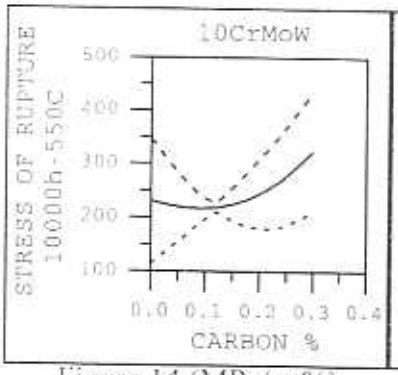

Figure 14 (MPa/wt%)

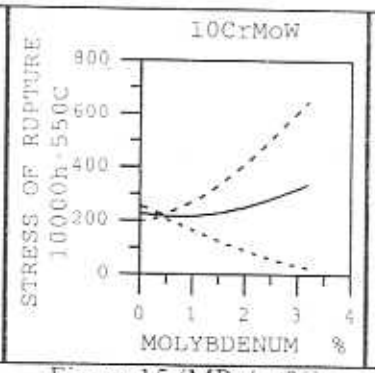

Figure 15 (MPa/wt%)

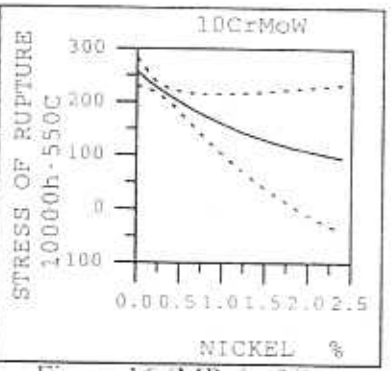

Figure 16 (MPa/wt%)

Carbon(Figure 14) : No convincing tendency.

Molybdenum (Figure 15) : As said in chapter two, this element presents a strong carbide-forming tendency which is interesting because as said in chapter one, the presence of fine and dispersed precipitates enhances creep resistance. However, no obvious trend was modelled by the neural network.

Nickel (Figure 16) : The nickel seems to be detrimental to the creep resistance. This effect of this element is well-known and explanations are currently debated. It is likely that nickel stabilises the M_6X precipitates which coarsen rapidly and become ineffective for creep resistance [Strang and Vodarek, 1997].

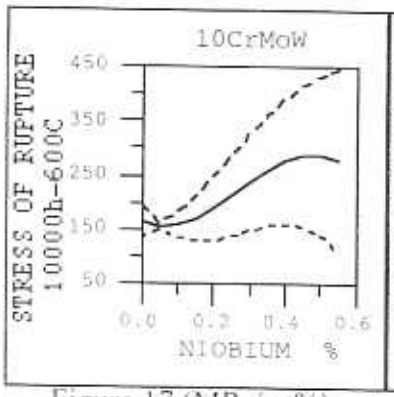

Figure 17 (MPa/wt%)

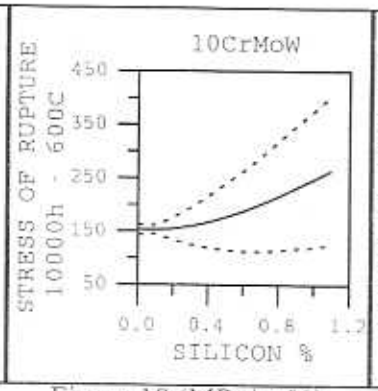

Figure 18 (MPa/wt%)

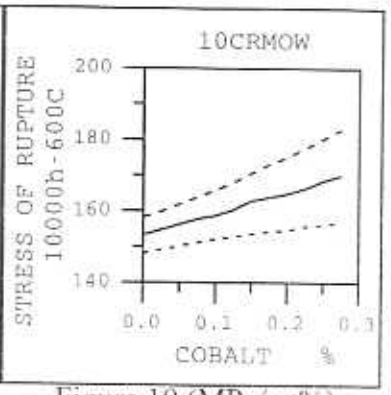

Figure 19 (MPa/wt%)

Niobium (Figure 17) : No convincing tendency.

Silicon and cobalt (Figure 18 and 19) : As stated in chapter two, both elements promote Laves phase precipitation. Assuming that this phase is beneficial to creep properties, this could explain the predicted behaviours. However, 10000 hours may not be a sufficient duration to have a significant amount of Laves phase particles [Foldyna and Kuboň, 1994]. As shown in chapter six (Figures 36 and 42), inverse tendencies were predicted for a greater duration. This suggests that actually Laves phase is detrimental to creep properties.

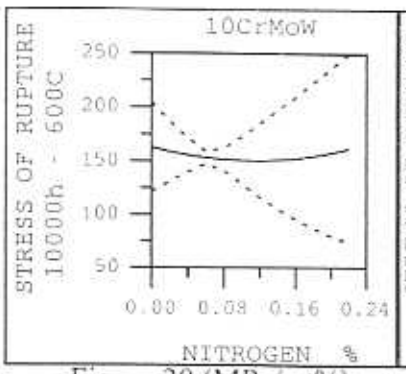

Figure 20 (MPa/wt%)

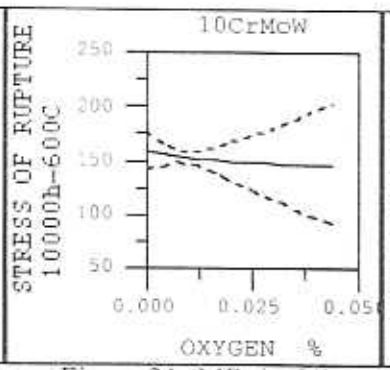

Figure 21 (MPa/wt%)

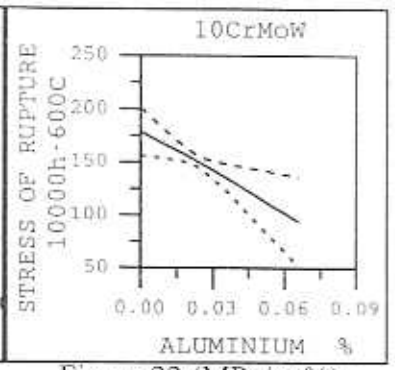

Figure 22 (MPa/wt%)

Nitrogen (Figure 20) : No convincing tendency.

Oxygen (Figure 21) : No convincing tendency.

Aluminium (Figure 22) : As said in chapter two, MX phase is of greatest importance for creep properties. Aluminium additions are detrimental to creep behaviour because the AlN phase forms instead of VN or NbN and this former phase coarsen rapidly whilst the latter remain fine and dispersed [Foldyna,*et al.*, 1997].

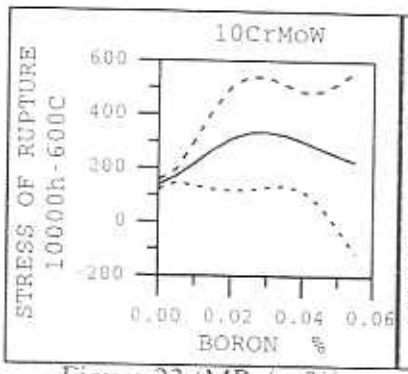

Figure 23 (MPa/wt%)

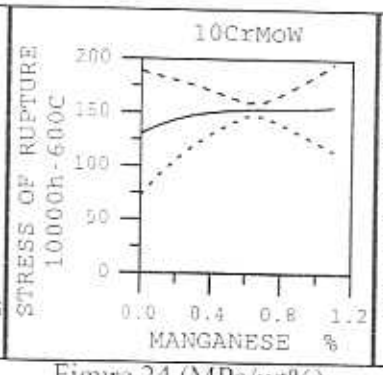

Figure 24 (MPa/wt%)

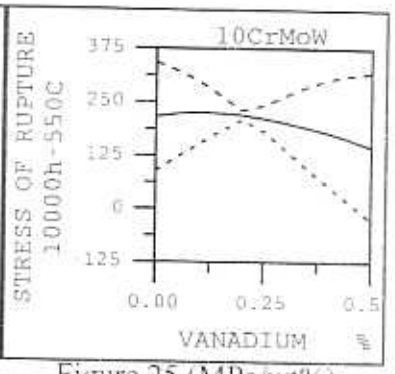

Figure 25 (MPa/wt%)

Boron (Figure 23) : As said in chapter two, its addition leads to increased precipitation at grain boundaries, and so impedes grain growth which is detrimental to mechanical properties. This effect of boron is modelled for very low concentrations (up to 0.006 wt%). Beyond this range, the error bars are too big to see any tendency, probably because of a lack of values in the database.

Manganese and Vanadium (Figure 24 and 25) : No convincing tendencies.

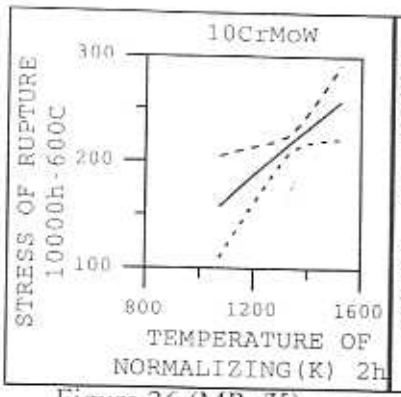

Figure 26 (MPa/K)

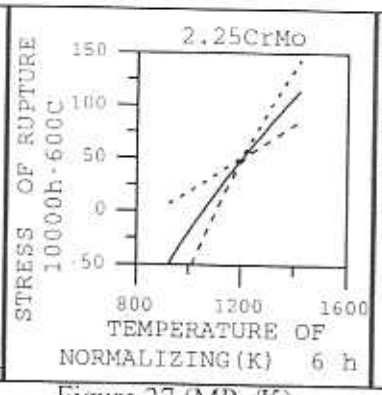

Figure 27 (MPa/K)

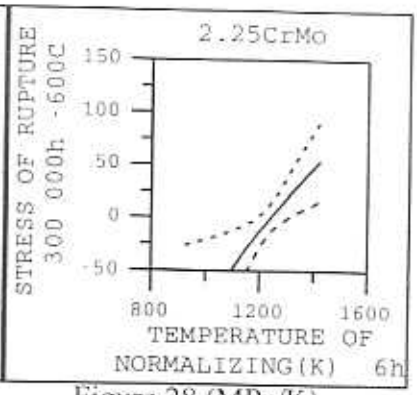

Figure 28 (MPa/K)

Temperature of normalising : (Figure 26 - 28) The duration of normalising was left at the value found in the database, 2 hours for the 10CrMoW steel, and 6 hours for the $2^1/_4$CrMo steel. This input is not really significant because it depends on the size of the tested sample which is unknown here. For both compositions, the higher the temperature, the better the creep resistance. In order to explain this, some thermodynamic calculations were performed using the National Physical Laboratory's Metallurgical and Thermodynamic Data Bank (MTDATA) [Hodson, 1989]. This package is capable of calculating phase equilibria for multi-component systems where many phases may be coexisting, by minimising the Gibbs free energy, whilst conserving mass.

These calculations were performed in both cases and indicated a full austenisation beyond 1200K. Supposing there is a kinetic effect which is not taken into account in the calculations, all carbides might be expected to be dissolved by 1300K. In both steels, the Nb contents are very low (0.01 and 0.005 wt%), and even if some niobium-rich MX precipitates remain in the matrix, their dissolution at only 1400K can not explain the observed behaviour. However some hypotheses can be considered as explanation :

(i) If full austenisation is not obtained and thus if ferrite and bainite are obtained at low $T\gamma$ (= temperature of normalising), i.e. just beyond 1200K, the creep resistance is improved because of the longer persistence of M_2X in ferrite than in bainite or martensite [Bhadeshia, 1992]

(ii) When $T\gamma$ increases, so do the grain size and hardenability. Indeed, the bigger the grain size, the easier it is to obtain martensite after cooling. Perhaps at low rates of cooling, ferrite and persisting M_2X are obtained.

(iii) If the grain size increases, the surface of grain boundaries decreases. Now, the Laves phase is known to form on grain boundaries [Foldyna and Kuboň,

1994]. Perhaps the decreasing surface of grain boundaries delays nucleation and formation of Laves phase, which could be beneficial assuming that Laves phase is detrimental to creep properties.

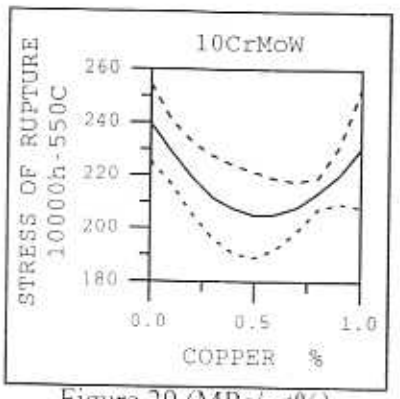

Figure 29 (MPa/wt%)

Copper : (Figure 29) The copper seems to be detrimental to creep resistance. Bain and Paxton, in *Alloying elements in steel*, (1961) explain that copper has a maximum solubility of less than 0.3 wt% in ferrite at 600°C. The copper dissolved at elevated temperatures is rejected as nearly pure copper particles at lower temperatures. According to Figure 29, copper addition are at first detrimental to creep resistance indicating that the copper particles coarsen and do not contribute significantly to precipitate strengthening.

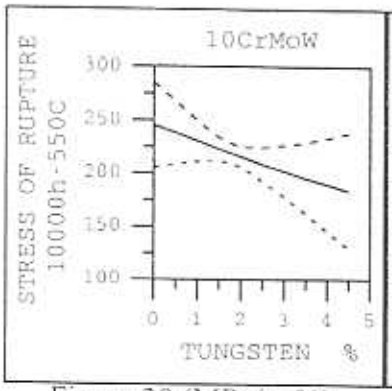

Figure 30 (MPa/wt%)

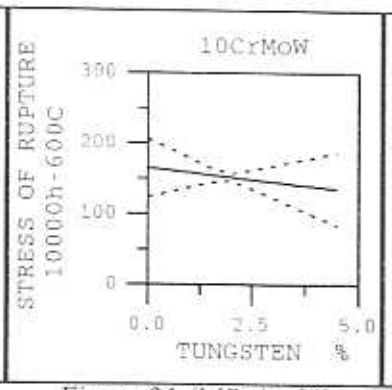

Figure 31 (MPa/wt%)

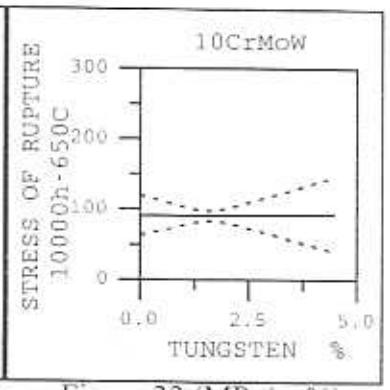

Figure 32 (MPa/wt%)

Tungsten : In Figure 30, tungsten addition seems to be detrimental to creep resistance. This behaviour is less significant at higher temperatures, and at 650°C the addition of tungsten seems to have no influence on the creep properties. As said in chapter two, tungsten promotes Laves phase formation. An explanation of this behaviour is presented below:

Assuming that Laves phase is detrimental to creep resistance, at 550°C this phase is stable and coarsens removing the tungsten from the matrix and so the solid solution strengthening effect of this element is reduced. At 600°C or 650°C Laves phase is less stable and an increasing content of tungsten does not require removal of so much tungsten from the matrix.

So the additions of tungsten become less detrimental to creep properties when the temperature increases, and have no effect at 650°C, as shown in Figures 30, 31 and 32.

The MTDATA calculations corroborate this explanation, so the equilibrium content of Laves phase decreases when the temperature increases, as shown in table 4.

Temperature	773K	823K	873K	923K	973K
content of Laves phase (mole %).	1.53	1.42	1.25	0.98	0.55

Table 4. [From MTDATA calculations]

These predictions suggest that the laves phase has a detrimental effect on the creep properties.

Other predictions concerning the effect of tungsten have been made and indicate an inverse tendency. Changes in the alloying element content cause this inversion of the behaviour. Indeed by removing copper from the 10CrMoW steel, the effect of tungsten was inversed, as shown in Figures 33 and 34.

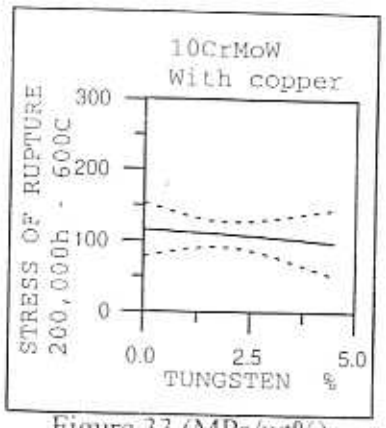

Figure 33 (MPa/wt%)

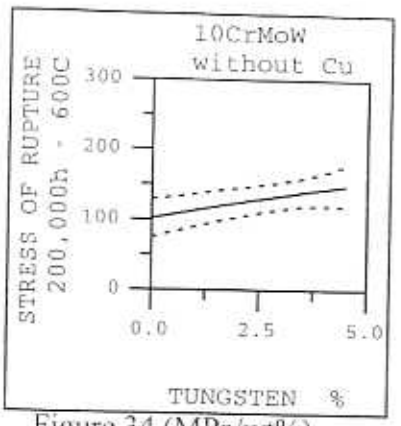

Figure 34 (MPa/wt%)

Copper may have a benificial effect on the nucleation of Laves phase [Schwind, Hättestrand and Andrén, 1996]. This could explain this inversion of tendency. When copper is present, there is formation of Laves phase which is detrimental to creep properties. When copper is removed, the tungsten remains in the matrix as a solid solution strengthener.

As seen in this chapter, the neural network allows many predictions to be made, which must be assessed according to physical behaviours. However, most of the predictions were not significant because of large error bars.

For the more significant tendencies, theoretical explanations were found. However, experimentation and metallurgical observation would be a good further way to assess the model.

CHAPTER SIX

DESIGN OF A NEW CREEP RESISTANT STEEL

a) First improvement of the 10CrMoW steel

Because the 10.6 Cr steel was already more creep resistant than the $2^1/_4$Cr steel, the former steel was therefore further improved.

The improvement in the creep resistance and size of the error bars were taken into account.

According to the graphs shown in figures 18, 19, and 22 the manganese and boron contents were set to 0 wt%, cobalt content to 0.125 wt% and aluminium content to 0.02 wt%.

In the steel obtained, the chromium content was modified and Table 5 was established. To choose the best chromium content, the value of the prediction minus the standard deviation was taken into account.

		TEMPERATURE	
		600°C	650°C
Cr in wt %	10.61	86.6	15.4
	7.0	103.0	13.4
	7.5	110.0	22.1
	8.0	113.0	27.7
	8.5	115.6	32.3
	9.0	114.2	34.9
	9.5	110.2	34.4
	10.0	101.5	28.4

Table 5:
{Predicted rupture stress - standart deviation} (MPa)
after $10^{5.7}$ hours (= about 56 years)

According to the values in Table 5, chromium content was set to 9 wt%.

This steel was theoretically tested. The results are presented in Figures 35 and 36. The new 9Cr steel is better than the 10CrMoW. However we are not sure that this is a local minimum, and this steel may be further improved.

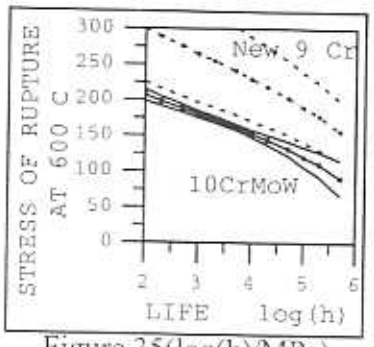

Figure 35(log(h)/MPa)

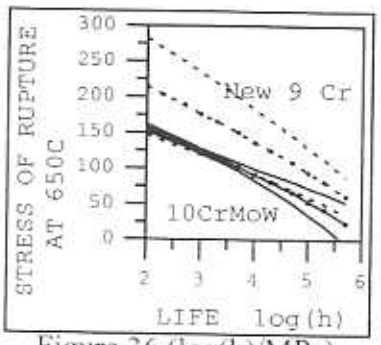

Figure 36 (log(h)/MPa)

Starting from this new 9Cr steel and following the graphs showing the rupture stress at 650°C and after $10^{5.5}$ (=315,000) hours vs different compositions an improvement was obtained. Eight inputs were changed.

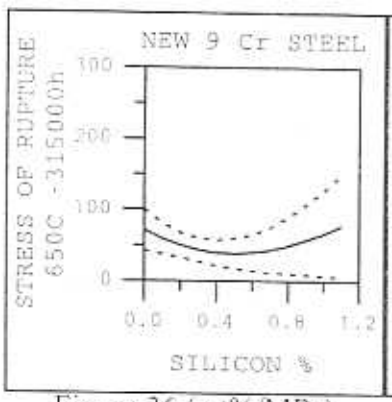

Figure 36 (wt%/MPa)

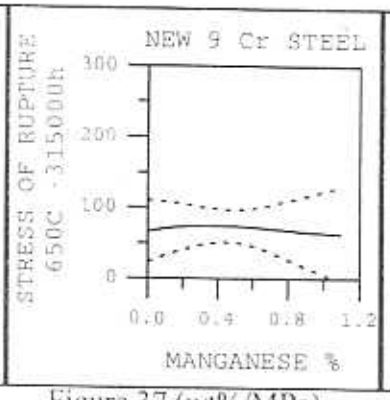

Figure 37 (wt%/MPa)

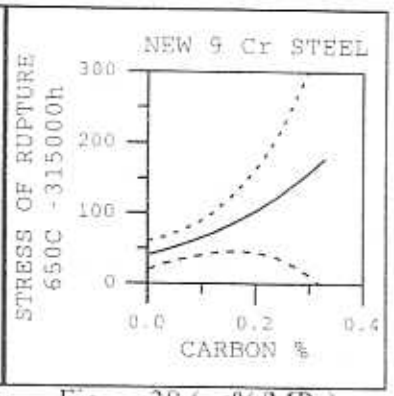

Figure 38 (wt%/MPa)

The silicon content was set to 0.48 wt% (Figure 36), manganese content left at 0 wt% (Figure 37), and carbon left at 0.12 wt%.

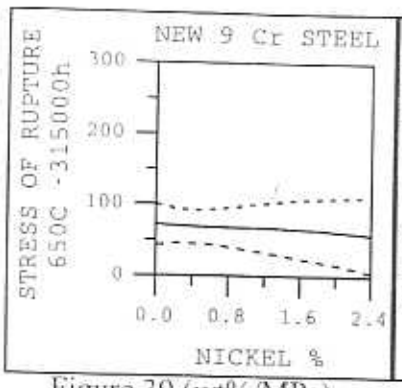

Figure 39 (wt%/MPa)

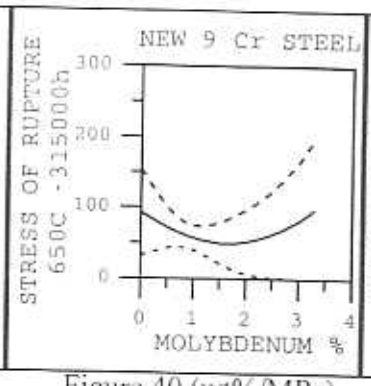

Figure 40 (wt%/MPa)

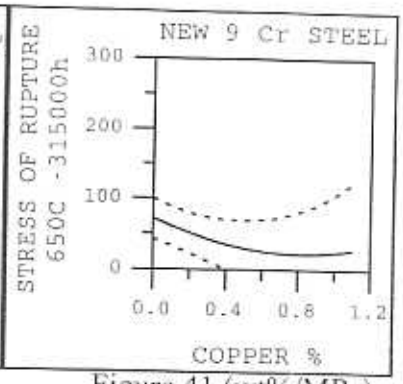

Figure 41 (wt%/MPa)

The nickel content was left at 0 wt%, tcopper at 0 wt% too, and molybdenum set to 0.75 wt%.

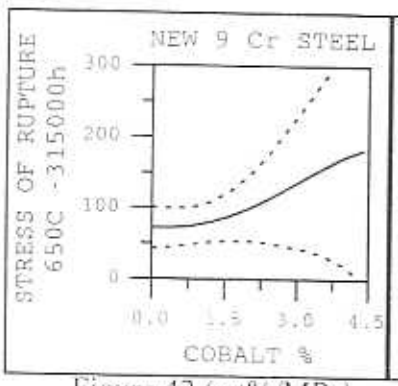

Figure 42 (wt%/MPa)

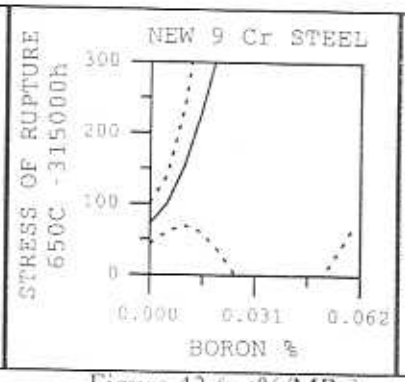

Figure 43 (wt%/MPa)

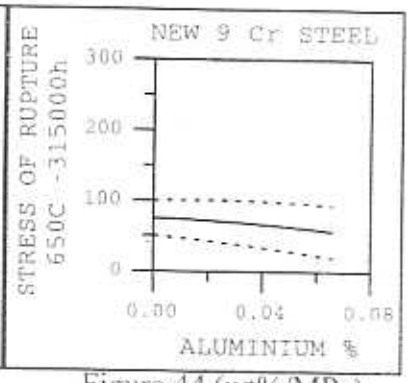

Figure 44 (wt%/MPa)

The cobalt content was set to 1.25 wt%, boron at 0.008 wt%, and aluminium set to 0 wt%.

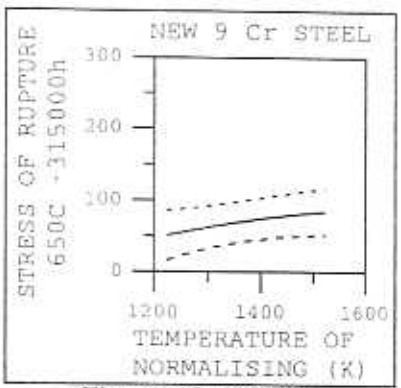

Figure 45 (K/MPa)

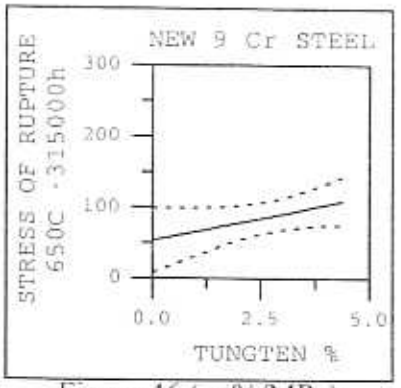

Figure 46 (wt%/MPa)

For tungsten and normalising temperature (Figures 45 and 46), the same trends as described in chapter five were found. The tunsten content was set to 3 wt% and the normalising temperature to 1473K.

STEEL	10.6CrMoW	STEEL A
Norm. temp.	1338K	1473K
Duration, hour	2h	2h
Cooling rate	in air	in air
Tempering T.	1043K	1043K
Duration, hour	4h	4h
Cooling rate	in air	in air
Annealing T.	1013K	1013K
Duration, hour	4h	4h
Cooling rate	in air	in air
C wt%	0.12	0.12
Si	0.05	0
Mn	0.64	0.48
P	0.016	0.016
S	0.001	0.001

STEEL	10.6CrMoW	STEEL A
Cr	10.61	9
Mo	0.44	0.75
W	1.87	3
Ni	0.32	0
Cu	0.86	0
V	0.21	0.21
Nb	0.01	0.01
N	0.064	0.064
Al	0.022	0
B	0.0022	0.008
Co	0.015	1.25
Ta	0.0003	0.0003
O	0.01	0.01
Re	0.0003	0.0003

Table 6

Table 6 shows the composition of this new steel which is called steel A and the composition of the 10CrMoW steel from which the improvement was developed.

Steel A was theoretically tested. The creep properties were noticeably improved at 600°C but the predicted behaviour at 650°C and $10^{5.7}$ hours was not significantly better than that of the 10.6Cr steel. The combination of two improvements probably gave worse properties.

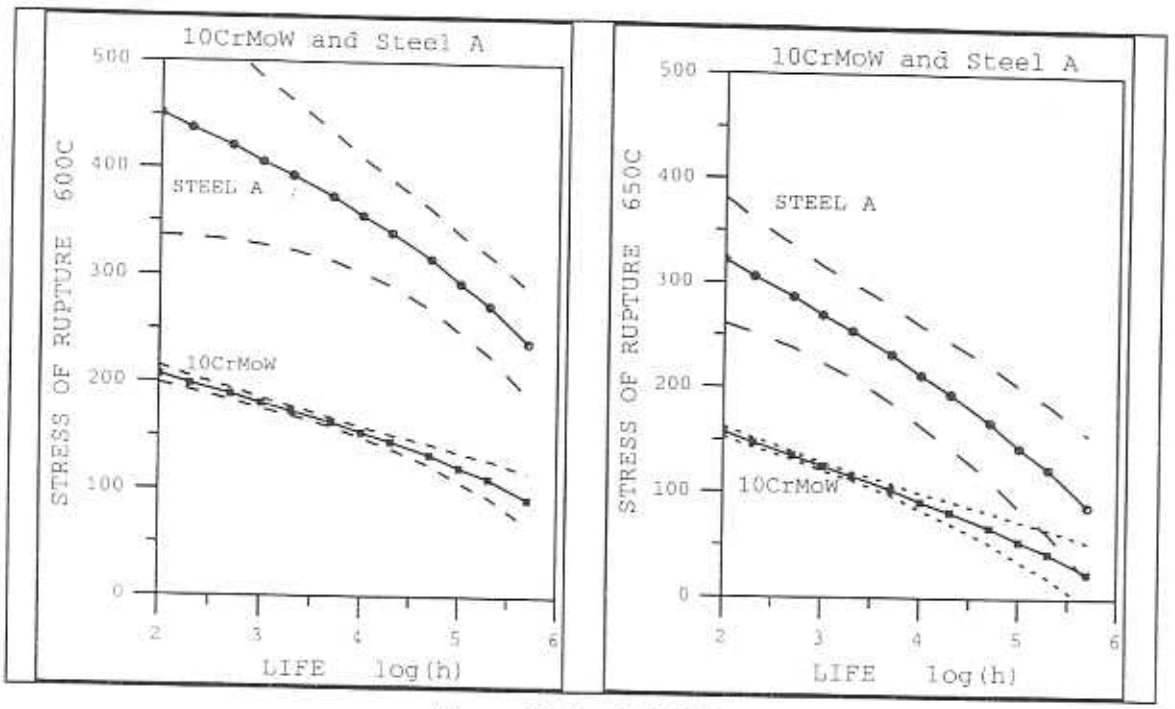

Figure 47.(log(h)/MPa)

b) Second improvement of the 10CrMoW steel

A second improvement was made from the same new 9Cr steel. The effect of compositional changes was predicted for all the inputs which had been changed or tested during the design of steel A, i.e. carbon, manganese, silicon, molybdenum, tungsten, nickel, copper, cobalt, aluminium and boron contents and normalising temperature. Variations in content were made step by step. Each time the change giving the best improvement in creep resistance and reasonable error bar size (about 22 MPa) was chosen, and the steel was re-tested with its new composition. To ensure that an improvement at 650°C and $10^{5.7}$ hours was obtained, these values were used as inputs to make predictions. Nine steps were necessary to obtain a local minimum, that is to say after nine steps, any change of content or heat treatment was detrimental to the creep behaviour of the steel obtained.

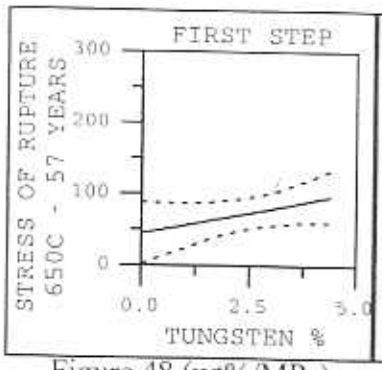

Figure 48 (wt%/MPa)

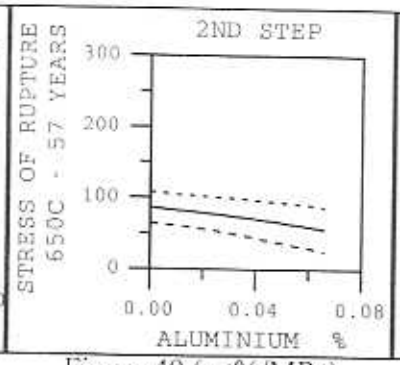

Figure 49 (wt%/MPa)

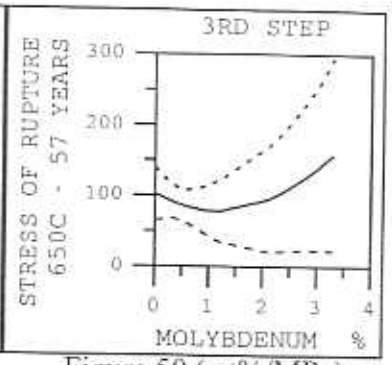

Figure 50 (wt%/MPa)

First step (Figure48): Tungsten content was set to 3 wt%.

Second step (Figure 49) : Aluminium content was set to 0wt%.

Third step (Figure 50) : Molybdenum content was set to 0.3 wt%.

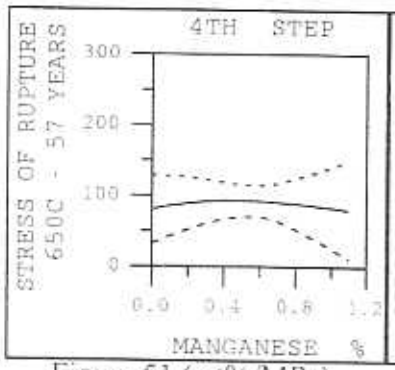

Figure 51 (wt%/MPa)

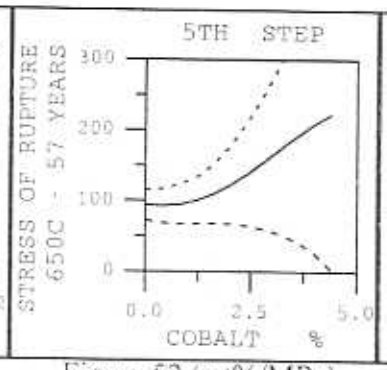

Figure 52 (wt%/MPa)

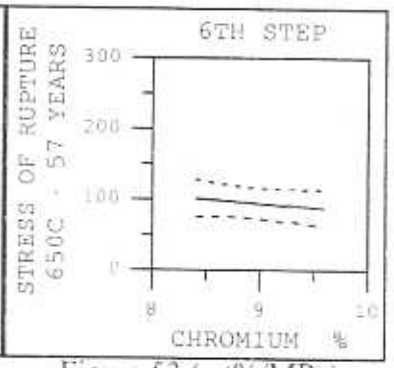

Figure 53 (wt%/MPa)

Fourth step (Figure 51) : Manganese content was set to 0.5 wt%

Fifth step (Figure 52) : The cobalt was removed (0wt%).

Sixth step (Figure 53) : The chromium content was lowered to 8.7 wt%.

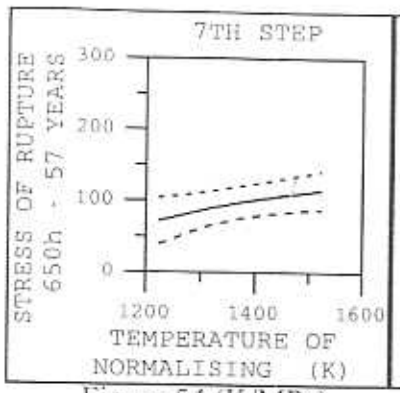

Figure 54 (K/MPa)

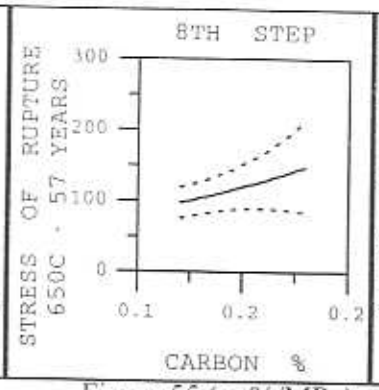

Figure 55 (wt%/MPa)

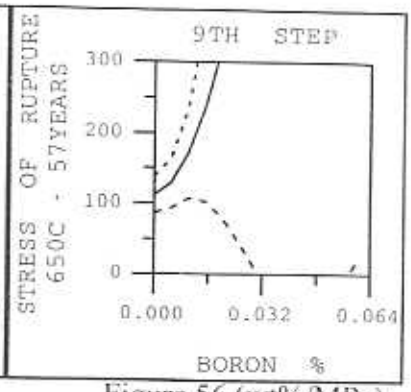

Figure 56 (wt%/MPa)

Seventh step (Fig. 54) : The highest temperature of the database was chosen that is to say 1453K.

Eighth step (Fig. 55) : The carbon content was fixed at 0.13 wt%.

Ninth step : According to the fist part of the figure 56, the boron content was set to 0.0003 wt%.

Steel B was obtained. Its predicted behaviour is much better than steel A at 650°C and for a longer time than 10,000 hours, which is really important for a power plant application (Figure 57).

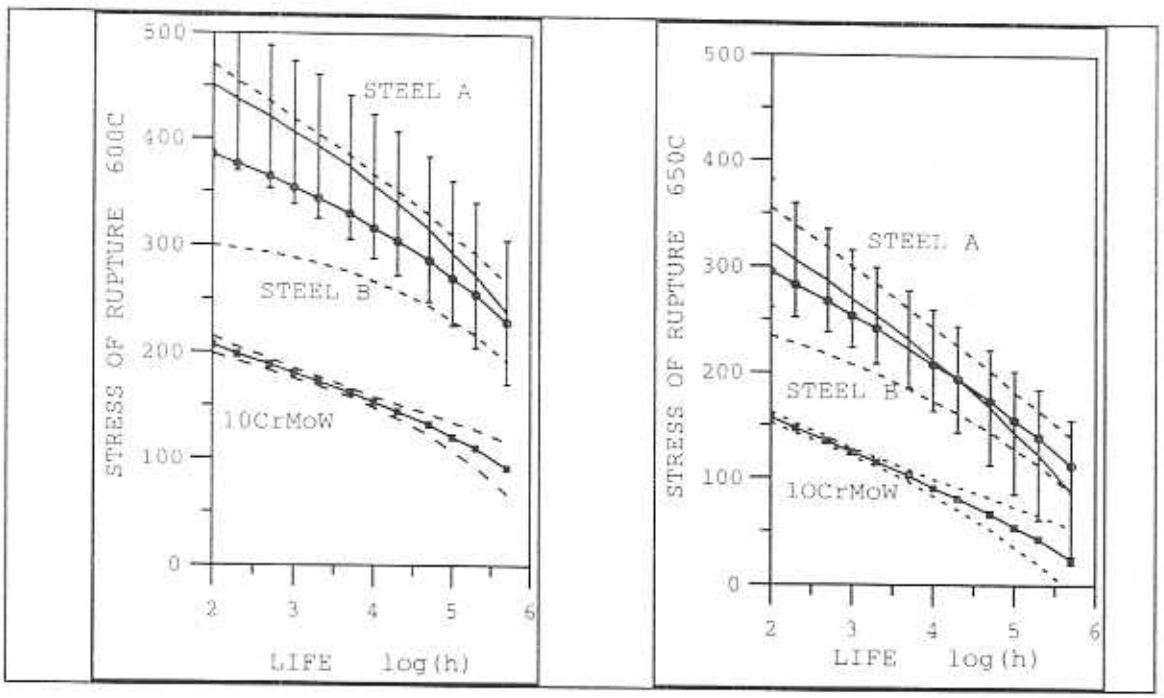

Figure 57 (log(h)/MPa)

If the predictions are relevant, this steel will withstand a 100MPa stress for about 36 years at a temperature of 650°C, that is really exceptional. The contents and heat treatments of the steels 10CrMoW A, B are given in Table 7.

STEEL	10CrMoW	A	B
Norm. temp.	1338K	1473K	1453K
Duration	2h	2h	2h
Cooling rate	in air	in air	in air
Tempering temp.	1043K	1073K	1073K
Duration	4h	4h	4h
Cooling rate	in air	in air	in air
Annealing temp.	1013K	1013K	1013K
Duration	4h	4h	4h
Cooling rate	in air	in air	in air
C w%	0.12	0.12	0.13
Si	0.05	0	0
Mn	0.64	0.48	0.5
P	0.016	0.0016	0.0016
S	0.001	0.001	0.001
Cr	10.61	9	8.7
Mo	0.44	0.75	0.3
W	1.87	3	3
Ni	0.32	0	0
Cu	0.86	0	0
V	0.21	0.21	0.21
Nb	0.01	0.01	0.01
N	0.064	0.064	0.064
Al	0.022	0	0
B	0.0022	0.008	0.008
Co	0.015	1.25	0
Ta	0.0003	0.0003	0.0003
O	0.01	0.01	0.01
Re	0.0003	0.0003	0.0003

Table 7

01793 785 327
01633 290011
4519
e-mail frandon@rmcs.cranfield.ac.uk.

c) Analysis of steels A and B

As reported in chapter two, δ-ferrite may form when the normalising temperature is too high. It is likely that this formation is not represented in the model because the heat treatments contained in the database were probably predetermined to prevent δ-ferrite from forming. The microstructural changes during the normalising were calculated with MTDATA software described in chapter five -c. As shown in Figure 58, beyond 1448K δ-ferrite forms in steel A. The normalising temperature was fixed at 1473K: it is too high. According to these thermodynamic calculations, the highest normalising temperature without δ-ferrite formation is 1448K. In the case of steel B (Figure 59), the δ-ferrite forms later, beyond 1473K, therefore the chosen normalising temperature (1453K) is correct. As shown in Figure 60, the 10CrMoW steel behaves similarly.

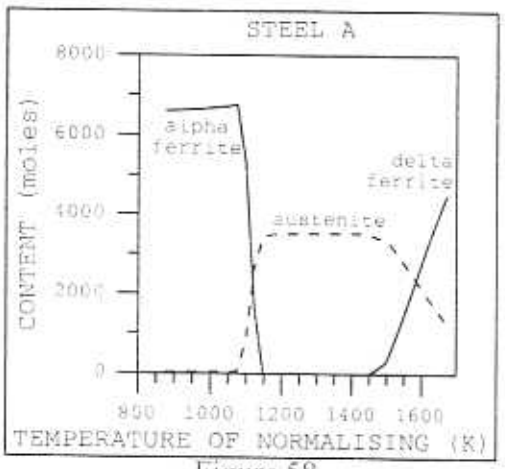

Figure 58

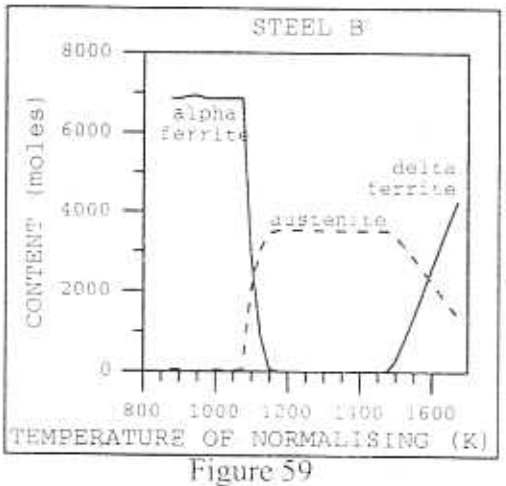

Figure 59

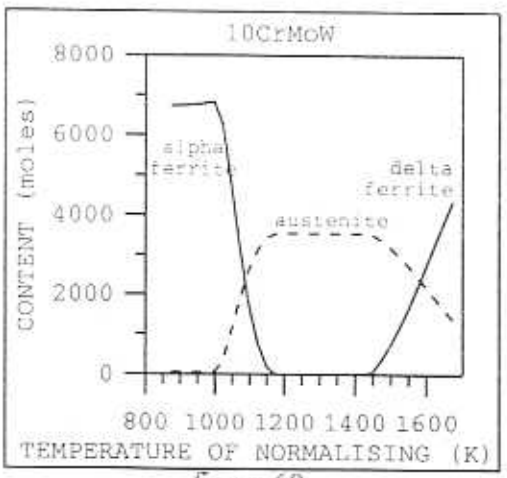

figure 60

The same thermodynamic calculations indicate the equilibrium contents of the main precipitates, $M_{23}C_6$ and Laves phase. These values are given in table 8. In each case, M_2X is not an equilibrium phase, MX exists but in very low amount.

	Temp.	873°K	923°K	973°K
10Cr steel	$M_{23}C_6$	2.69	2.69	2.68
	Laves p.	1.13	0.79	0.24
steel A	$M_{23}C_6$	2.73	2.72	2.71
	Laves p.	2.64	2.34	1.88
steel B	$M_{23}C_6$	2.94	2.94	2.92
	Laves p.	2	1.65	1.13

Table 8.

Laves phase is an equilibrium phase and is detrimental to creep properties. But the formation of Laves phase is not proved: the kinetic of formation must be taken into account. That is why another software program was used to predict the developpement of micostructure under service conditions. It is J.D. Robson's program named *kinetics.for* [Robson, 1996;Robson and Bhadeshia, 1996]. Although Laves phase is an equilibrium phase, this kinetic model does not predict any formation of this intermetallic precipitate in steel A or B at 600°C or 650°C (Figure 61 -64). These temperature are probably too high for the formation of Laves phase. The same predictions were made for the 10CrMoW steel. At 600°C (Figure 65), the microstructural changes are similar in spite of a smaller amount of M_2X precipitate. At 650°C (Figure 66), Laves phase is predicted to form after more than 5 years. This phenomenon probably causes bad creep properties of this steel.

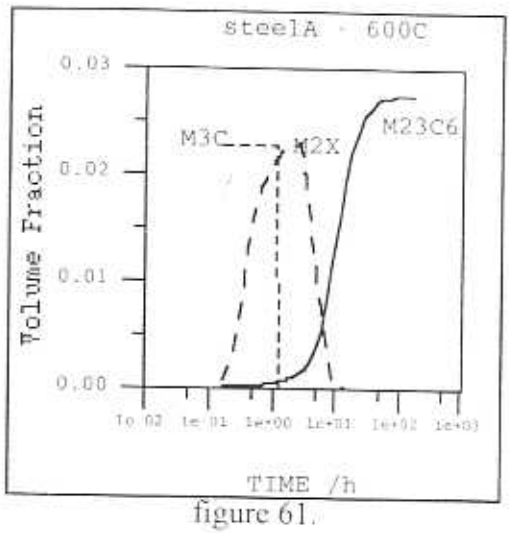

figure 61.

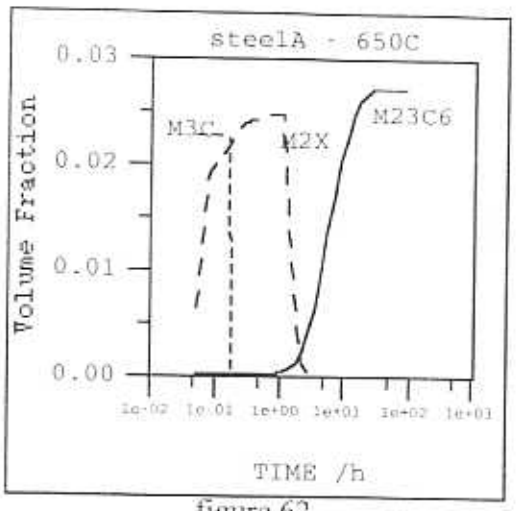

figure 62

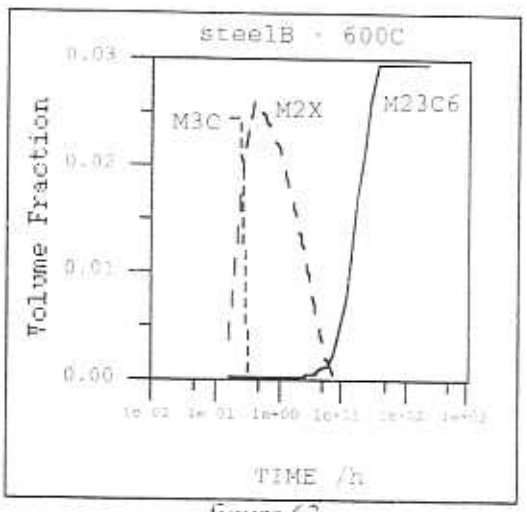

figure 63

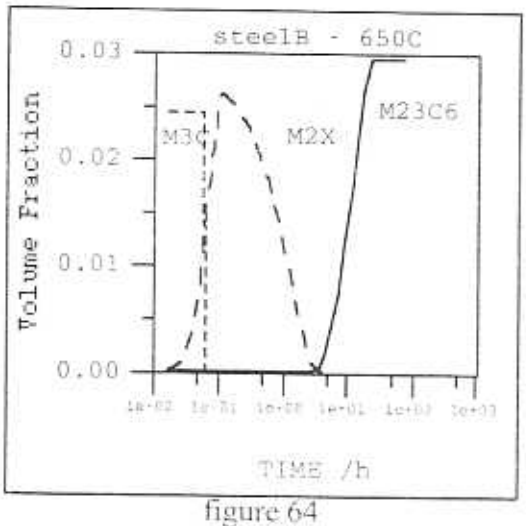

figure 64

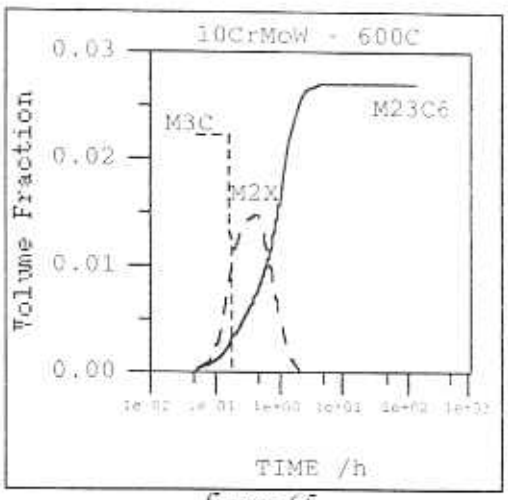

figure 65

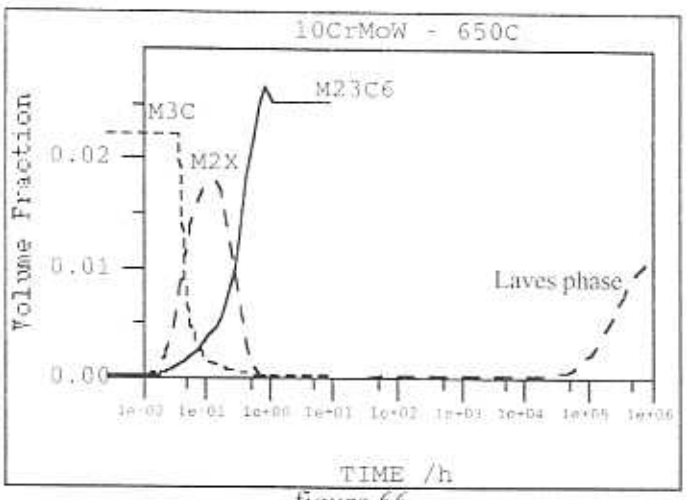

figure 66

These microstructural predictions do not prove the good creep behaviour of the steel A and B but assuming that Laves phase is detrimental to creep properties, the absence of this intermetallic phase seems to be in accordance with the predicted and expected creep properties.

d) Comparison with NF616 and NF12 [Ohgami *et al.*, 1997]

Nippon Steel developed two high creep resistant steels named NF616 and NF12. Their composition and those of steels A and B are given in table 9.

STEEL	A	B	NF616	NF12
C w%	0.12	0.13	0.10	0.08
Si	0	0	0.25	0.2
Mn	0.48	0.5	0.5	0.5
Cr	9	8.7	9	11
Mo	0.75	0.3	0.5	0.15
W	3	3	1.8	2.6
Ni	0	0	<0.4	<0.6
V	0.21	0.21	0.20	0.20
Nb	0.01	0.01	0.07	0.07
N	0.064	0.064	0.050	0.050
B	0.008	0.0003	0.002	0.004
Co	1.25	0	0	2.5

Table 9

As can be seen, the general trends in composition are similar: high tungsten content, low silicon content, similar chromium, manganese, vanadium, nitrogen and boron contents and absence of aluminium and copper.

This is the best proof of the efficiency of the neural network modelling.

CONCLUSIONS AND FURTHER WORK

During this work, a neural network was trained to model the creep properties of steel. A database of 2066 creep rupture test results was used. After the training, the neural network was able to reproduce accurately the behaviour of any steel found in the database. In some cases and in particular when one of the contents of the tested steel was out of the range of the database, large error bars were obtained and no convincing prediction could be made.

This suggests one of the possible area for further work. Indeed, by increasing the size of the database, and by including other kinds of steels such as steels in which chromium content is low or between 2.5 and 8 wt%, the model could be extended to predict behaviours of a greater number of steels and with a greater accuracy.

The model has been used to design two very creep resistant steels. Starting from a typical 10CrMoW steel, the main composition changes consist of removing Al and Ni and elements which promote formation of Laves phase - silicon, copper, cobalt. Chromium and molybdenum contents were lowered. In spite of increasing tungsten content, all these changes suggest that Laves phase is detrimental to creep properties.

The compositions of steels A and B are similar to that of two creep resistant steels named NF616 and NF12. This proves the power and the effectiveness of the neural network modelling.

In conclusion, even if the compositions of theoretically created steels A and B seem to be reasonable and not in contradiction to good creep properties, these steels must be manufactured, experimentally tested and analysed. This could be another subject for further work.

REFERENCES

Bain, E.C. and Paxton, H.W.: 'Alloying Elements in Steel', Am. Soc. Met. (1966) p. 78

Baker, R.G. and Nutting J.: *J. Iron Steel Inst.* **192** (1959) p. 257-268

Balluffi, R.W., Cohen, M. and Averbach, B.L.: *Trans Am. Soc. Met.* **43** (1951) p. 497-526

Bhadeshia, H.K.D.H.: 'Bainite in Steels', Institute of Materials, London (1992)

Bjärbo, A.: 'Microstructural Changes in a 12% Chromium Steel during Creep' Report, Royal Institute of Technology, Stockolm, Sweden (1994) p.11

Evans, R.W. and Wilshire, B.: 'Creep of Metals and Alloys', the Institute of Metals (1985) p. 189

Foldyna, V. and Kuboň, Z.:'Creep Resistant Chromium Steels - Metallurgical Understanding', COST 501, Round 3, WP 11 (1994)

Foldyna, V., Kuboň, Z., Jakovová and Vodárek, V.: ' Development of Advanced High Chromium Ferritic Steels', in Microstructural Development and Stability in High Chromium Ferritic Power Plants Steels, Edited by A. Strang & D.J. Gooch, The Institute of Materials, London (1997) p.74

Frost H.J. and Ashby, M.F.: 'The Plasticity and Creep of metals and ceramics', Pergammon Press, Oxford (1982)

Greenwell, B.S. and Beech, S.M.: "The Rupture Ductility of High Alloy Ferritic Steels' power industry conference, Liege, Belgium (1994)

Hodson, S.M.: MTDATA - Metallurgical and Thermochemical Databank, National Physical Laboratory, Teddington, U.K. (1989)

Hosoi, Y., WadeN. and Urita T.: *Trans Iron Steel Inst. Japan* **26** (1986) B-30

Irvine K.J., and Pickering F.B.: 'High-Strength 12% Chromium Steels' (1964)

Janovec, J., Vyrostkova, A. and Svoboda, M.: *Met. Trans A* **25A** (1994) p. 267-275

Kuo, K.: *J. Iron Steel Inst.* **173** (1953) p. 363-375

MacKay, D.J.C.: *Neural Computation* **4** (19920 p. 415-472

Mayer, K.H., Crejak, H., Hofer, P., Letofsky, E. and Schuster, F.: ' Evolution of structure and Properties of 10% Cr Steel Casting', in Microstructural Development and Stability in High Chromium Ferritic Power Plants Steels, Edited by A. Strang & D.J. Gooch, The Institute of Materials, London (1997) p.105

Nickel, H., Ennis, P.J., Wachter, O.: 'The Effect of Heat Treatment on the Microstructureand Creep properties of 9Cr-0.5Mo-1.8W Steel', Am. Soc. Met./JSMEPressure Vessels and Piping Conference, Honolulu, Hawaii (1995)

Norton F.H.: 'Creep of Steel at High Temperatures' Mc-Graw-Hill, New-York (1929) p. 67

Ohgani, M., Hasegawa, Y. and Naoi, H.: 'Development of 11CrMoWCo Heat Resistant Steel for Fossil Thermal Plants' IMechE C522/012 (1997) p. 120

Pickering, F.B. and Vassiliou, A.D.: *Metals Technology* (October, 1980) p.409-413

Reed-Hill, R. and and Abbachian, R.: 'Physical Metallurgy Principles", PWS Kent, Boston (1992) p. 844

Robson, J.D.: Ph.D. Thesis, University of Cambridge, U.K. (1996).

Robson, J.D. and Bhadeshia H.K.D.H.: ' Modelling the Development of Microstructure in Power Plant Steels', in Microstructural Development and Stability in High Chromium Ferritic Power Plants Steels, Edited by A. Strang & D.J. Gooch, The Institute of Materials, London (1997) p.179

Sanderson, S.J.: 'Mechanical Properties and Metallurgy of 9%Cr-1Mo Steel', Ferritic steels for High Temperature Applications, Am. Soc. Met. (1983) p. 85-99

Schwind, M., Hättestrand, M. and Andrén H.-O.: 'High Resolution Microanalysis of Ferritic Steel HCM12A' Sweden (1996)

Senior, B.A.: *Mat. Sci. Eng.* **119A** (1989)

Shaw, S.W.K. and Quarrell, A.G.: *J. Iron Steel Inst.* **185** (1957) p. 10-22

Spiradek, K., Bauer, R and Zeiler G. : Materials for advanced Power Engineering, Liege, Belgium (1994) p. 251-262

Strang, A. and Vodárek, V.: ' Precipitation processes in Martensitic 12CrMoVNb Steels During High Temperature Creep', in Microstructural Development and Stability in High Chromium Ferritic Power Plants Steels, Edited by A. Strang & D.J. Gooch, The Institute of Materials, London (1997) p.31

Straub, S., Meier, M., Ostermann, J. and Blum, W.: *VGB Kraftwerkstechnik* **73** (1993) p. 646-653

Takeda, Y. and Masuyama, F.: 1st International Conference on Heat Resisting Materials, Wisconsin, U.S.A. (1991)

Thomson, R.C.: Ph.D. Thesis, University of Cambridge, U.K. (1992).

Vanstone R,W.: 'Microstructure and Creep mechanisms in advanced 9-12% Cr Creep Resisting Steels', Materials for advanced Power Engineering, Liege, Belgium (1994)

Watcher, O. and Ennis, P.J.: Ph.D. Thesis, Technische Hochschule, Aachen, Germany (1995) p. 6-16

Woodhead and Quarrell, A.G.: *J. Iron Steel Inst.* **203** (1965) p. 605-620

Yakel, H.L.: *International Metals Reviews* **30(1)** (1985) p. 17-40

APPENDIX 1

LOCALISATION OF THE GRAPHS OF THIS REPORT IN THE SUN-FILES

All files are in the folder brun: */huge/users/brun*

Table 1; *brun/predictions/minmaxtaka*

Figure 8. a: *brun/training/graphte.spy*

Figure 8. b:*brun/training/graphsn.spy*

Figure 9: *brun/committee/graphte.spy*

Figure 10. a: *brun/committee/graph1st.spy*

Figure 10. b: *brun/committee/graphexpdco.spy*

Figure 11: *brun/committee/graphsw.spy*

All the outprdt'i' foders, where 'i' is included between 1 and 32, are in the *brun/predictions/..* folder. If you want to find the name of the graph, go to the indicated folder and read the file named *info*.

Figure 12. a: *outprdt6*

Figure 12.b: *outprdt7*

Figure 12. c: *outprdt7*

Figure 13. a: *outprdt29*

Figure 13. b: *outprdt29*

Figure 14: *outprdt6*

Figure 15: *outprdt6*

Figure 16: *outprdt6/*

Figure 17: *outprdt7*

Figure 18: *outprdt7*

Figure 19: *outprdt7*

Figure 20: *outprdt7*

Figure 21: *outprdt8*

Figure 22: *outprdt8*

Figure 23: *outprdt8*

Figure 24: *outprdt8*

Figure 25: *outprdt6*

Figure 26: *outprdt6*

Figure 27: *outprdt14*

Figure 28: *outprdt14*

APPENDIX 2

LOCALISATION OF THE GRAPHS OF THIS REPORT IN THE DISK (FREDGRAPHS) AND PT TRIGGER/ B-TEAM/FRED/FREDGRAPHS

Figure 8. a: *graphte.spy*

Figure 8. b:*graphsn.spy*

Figure 9: *graphtecom.spy*

Figure 10. a: *graphcom.spy*

Figure 10. b: *graph1st.spy*

Figure 11: *graphsw.spy*

Figure 12. a: *10Crgraph0.spy*

Figure 12.b: *10Crgraph1.spy*

Figure 12. c: *10Crgraph2.spy*

Figure 13. a: *3Crgraph.spy*

Figure 13. b: *9Crgraph.spy*

Figure 14: *Cgraph1.spy*

Figure 15: *Mograph1.spy*

Figure 16: *Nigraph1.spy*

Figure 17: *Nbgraph1.spy*

Figure 18: *Sigraph1.spy*

Figure 19: *Cograph1.spy*

Figure 20: *Ngraph1.spy*

Figure 21: *Ograph1.spy*

Figure 22: *Algraph1.spy*

Figure 23:*Bgraph1.spy*

Figure 24: *Mngraph1.spy*

Figure 25: *Vgraph1.spy*

Figure 26: *NTgraph4.spy*

Figure 27: *NTgraph1.spy*

Figure 28: *NTgraph3.spy*

Figure 29: *Cugraph1.spy*

Figure 30:*Wgraph1.spy*

Figure 31: *Wgraph4.spy*

Figure 32: *Wgraph6.spy*

Figure 33: *Wgraph10.spy*

Figure 34: *W-Cugraph1.spy*

Figure 35. a : *SteelII1.spy*

Figure 35. : *SteelII2.spy*

Figure 36:*Sigraph2.spy*

Figure 37: *Mngraph2.spy*

Figure 38: *Cgraph2.spy*

APPENDIX 3

HOW USE THE NEURAL NETWORK TO DO SOME PREDICTIONS.

All the useful files and FORTRAN program are in the folder */huge/users/brun/predictions*

1) Go to this folder.

2) Create a folder named *outprdt.*

3) Create a document named *test.dat*

4) In this file named *test.dat*, write the composition, the heat treatments and the test duration and temperature of the steel you want creep resistant to be predicted. You must fill the 37 columns which must be separated by a tabulation. The columns must be in the following order:

1) log(creep rupture time(h))
2) temperature(K)
3) C
4) Si
5) Mn
6) P
7) S
8) Cr
9) Mo
10) W
11) Ni
12) Cu
13) V
14) Nb
15) N
16) Al
17) B
18) Co
19) Ta
20) O
21) Normalising Temp.
22) Normalising Time

23) Cooling rate of Normalise in furnace (0 or 1)
24) Cooling rate of Normalise in air (0 or 1)
25) Cooling rate of Normalise for oil quench (0 or 1)
26) Cooling rate of Normalise for water quench (0 or 1)
27) Tempering Temp.
28) Tempering Time
29) Cooling rate of Tempering in furnace (0 or 1)
30) Cooling rate of Tempering in air (0 or 1)
31) Cooling rate of Tempering for oil quench (0 or 1)
32) Cooling rate of Tempering for water quench (0 or 1)
33) Anealing Temp.
34) Anealing Time
35) Cooling rate of Anealing in furnace (0 or 1)
36) Cooling rate of Anealing in air (0 or 1)
37) Re

The simplest way to write a test.dat file is to copy and paste a line of an old test.dat file (in one of the outprdt'i' files) and to change its values.

5) When *test.dat* is completed, count its number of lines (= number of rows), and change the values in the *normtest.for*, *treatout.for*, *gencom.for* and *spec.g* files.

In normtest.for: line 15: irow='number of lines in test.dat'.

In treatout.for: line 14: irow='number of lines in test.dat'.

In gencom.for: line 64: irow='number of lines in test.dat'.

In spec.g: lines 18 to 22: **Nrows** indicates where you have to type the 'number of lines in test.dat':

Data_files(inputs_targets)	normtest	outran.g
Number_data	**Nrows**	
Train_from_1_to_this		1
Test_set_1	1	**Nrows**
Test_set_2	1	**Nrows**

6) Run the *normtest.for* program which normalises the inputs and write them in *normtest:* type:

f77 normtest.for (return)
a.out (return)

7) Run the neural network program:type:

csh run.gen (return)

8) Run the *gencom.for* program: type:

f77 gencom.for (return)
a.out (return)

The normalised output are written in the *com.dat* file.

9) Run the *treatout.for* program which unnormalises the outputs and writes them in *unnorm_com* file.

f77 treatout.for (return)
a.out (return)

In unnorm_com are written 4 columns:

1) Predicted value
2) Error (65% confident)
3) Predicted value + Error
4) Predicted value - Error

10) Move the *com.dat*, *test.dat*, and *unnorm_com* files from the predictions to the *outprdt* folder. You can now use spyplot to draw your graphs.